Institut für Geographie
Lehrstuhl für Physische Geographie
und Quantitative Methoden

Universität Augsburg
Institut für Geographie

Masterarbeit

im Studiengang Klima- und Umweltwissenschaften

Spatial and temporal variability of stable water isotopes in firn cores from Dronning Maud Land, East Antarctica

vorgelegt von

Alexandra Zuhr

in Kooperation mit dem

ALFRED-WEGENER-INSTITUT
HELMHOLTZ-ZENTRUM FÜR POLAR- UND MEERESFORSCHUNG

Gutachter: Prof. Dr. Jucundus Jacobeit

Betreuer: Thomas Münch, Dr. Thomas Laepple

Potsdam, 2018

Abstract

The isotopic composition of ice sheets is a temperature proxy and allows the reconstruction of past climates. However, the accuracy of the reconstructions is dependent on the knowledge about local processes affecting and altering the climatic signal. This thesis investigates the spatial and temporal variability of stable oxygen isotopes in firn cores from Dronning Maud Land, East Antarctica in order to infer reliable conclusions on the past climate in this region.

In particular, different sampling, measuring and processing techniques can influence the resulting timeseries. The used sample types are samples from firn cores as well as samples from snow pits and trenches which differ in sample collection and storage. Individual snow samples have to be measured discretely whereas core segments can alternatively also be measured continuously in a CFA system. Both ways allow the determination of isotopic ratios in laser spectrometers; of which the raw data require a post-run correction and a calibration to international standards. In this thesis, discretly and continuously measured firn cores as well as samples from snow pits and snow trenches are analysed. For this, different post-run corrections schemes are compared. The results show that there are no significant discrepancies between the mentioned methods.

Further on, eleven firn cores with horizontal distances up to 15 km are analysed in a resolution of 50 cm to a depth of 30 m covering the period from 1809 to 2012. Firstly, each core is analysed individually and mean annual accumulation rates are calculated. A general increase during the last 50 years is observed, although individual profiles deviate from the mean trend. Secondly, a stacked data set is developed to compensate for non-climatic effects and to improve the signal-to-noise ratio. Considering the last 50 years, we find a positive trend of 0.16 °C/decade in the stacked isotopic timeseries. Although the imprint of climate signals in snow and firn is still not completely understood, the increase in isotopic ratios and the derived rise in temperature are robust due to the combination of several profiles. A comparison with a data set covering the period from 1000 to 1950 CE leads to the suggestion that the unusual high values during the last decades might be an indication for an anthropogenic influence on the climate.

Zusammenfassung

Die isotopische Zusammensetzung eines Eisschildes lässt auf vergangene klimatische Bedinungen schließen. Die Genauigkeit dieser rekonstruierten Daten ist dabei abhängig von lokalen Prozessen, die vor, während oder nach der Schneeablagerung das Klimasignal beeinflussen und verändern. Die vorliegende Arbeit untersucht die räumliche und zeitliche Variabilität stabiler Sauerstoffisotope in Firnkernen aus Dronning Maud Land, Ostantarktis mit dem Ziel eine verlässliche Aussage über das vergangene Klima abzuleiten.

Die in dieser Arbeit verwendenten Proben stammen aus Firnkernen, Schneeprofilen und Schneegräben. Die analysierten Zeitreihen können beeinflusst sein durch unterschiedliche Methoden in der Probennahme, in der Messung der Isotopien und der Datenprozessierung. Proben von Firnkernen unterscheiden sich von losen Schneeproben sowohl in der Probennahme als auch in der -lagerung. Segmente eines Firnkerns können kontinuierlich in einem CFA System beprobt und gemessen werden oder alternativ in diskrete Proben geschnitten und, wie Proben aus Schneeprofilen, diskret gemessen werden. Unabhängig von der Beprobung wird dann die isotopische Zusammensetzung in einem Laserspektrometer bestimmt, dessen Rohdaten korrigiert und an internationale Standards angepasst werden müssen. In dieser Arbeit wurden diskret und kontinuierlich gemessene Firnkerne als auch Proben aus Schneeprofilen und -gräben analysiert, dabei wurden auch verschiedene Prozessierungsmethoden verglichen. Die erzielten Ergebnisse zeigen, dass es keine signifikanten Unterschiede zwischen den genannten Methoden gibt.

Weiterhin wurden elf Firnkerne mit einer Auflösung von 50 cm bis zu einer Tiefen von 30 m untersucht. Die Daten decken die Zeitspanne von 1809 bis 2012 ab. Die Standorte der Firnkerne sind zwischen einigen Metern und 15 km voneinander entfernt. Zunächst wurde jeder Kern einzeln analysiert. Hierbei wurden u. a. mittlere jährliche Akkumulationsraten berechnet und ein Anstieg in den letzten 50 Jahren festgestellt, welcher jedoch nicht in jedem Datensatz zu erkennen ist. Weiterhin wurden alle elf Zeitreihen zu einem Datensatz gemittelt um nicht-klimatische Einflüsse im Signal zu minimieren. Die isotopische Zusammensetzung des gemittelten Datensatzes zeigt für die letzten 50 Jahre einen positiven Trend, der umgerechnet einen Temperaturanstieg von 0.16 °C/Dekade andeutet. Bis heute ist noch nicht vollständig geklärt, wie genau sich das Klimasignal im Schnee ablagert. Der Trend, der in dieser Arbeit berechnet wurde, ist aufgrund der Mittelung über elf Firnkerne dennoch aussagekräftig. Ein Vergleich mit einer Datenreihe, die die Zeitspanne von 1000 bis 1950 abdeckt, zeigt, dass die stark positiven Werte ungewöhnlich sind und ein möglicher Indiz für einen anthropogenen Einfluss auf das Klima sein können.

Contents

List of Figures

List of Tables

List of Abbreviations

AP Antarctic Plateau

AWI Alfred Wegener Institute for Polar and Marine Research

AWS automatic weather station

CFA Continuous Flow Analysis

CRDS Cavity-Ring Down Spectroscopy

DEP Dielectric Profiling

DML Dronning Maud Land

IRMS Isotope Ratio Mass Spectrometry

PSD power spectral density

RMSD root mean square deviation

SLAP Standard Light Antarctic Precipitation

VSMOW Vienna Standard Mean Ocean Water

w. eq. water equivalent

1. General introduction

Paleoclimatology is the science of studying past changes in climate over the entire history of the Earth, aiming at an understanding of the Earth's climate system. Since instrumental observations of climate parameters (e. g. temperature) started only about 150 years ago (National Research Council, 2006), most of the information on past changes are derived from indirect proxy data, i. e. from environmental indicators sensitive to changes in certain climatic variables. These data are stored in globally distributed environmental archives (such as ice sheets, marine sediments, corals and tree rings) and thus allow comprehensive and detailed estimates of climate variability during the past millennial (Marcott et al., 2013; National Research Council, 2006).

The climate in polar regions is determined by cold conditions and the presence of snow- and ice-covered areas. Strong seasonal variations of incoming solar radiation influence the climate and lead to very low temperatures, especially during winter. The climate is very sensitive to changes due to self-amplifying feedbacks once an effect is triggered (IPCC, 2001); changes are thus particularly pronounced in these areas and will affect other regions of the world. It is therefore important to study proxy data of the last millennium from polar regions, which are the key region for climate change, in order to distinguish between natural variability and anthropogenic forced warming.

Ice sheets represent one of the main reservoirs in the global climate system archiving information on past climatic conditions (EPICA community members, 2004). Studies in polar regions use parameters as the isotopic composition of snow and ice as temperature proxies. Isotopic compositions preserve the climatic conditions during the snow formation and store these information (IPCC, 2013). Temporal and spatial patterns on large scales as e. g. glacial-interglacial cycles are very well documented in the ice (e. g. Schilt et al., 2010). However, on short scales the reconstruction is still subject to great uncertainty because it is yet not completely clear, how exactly and to which extent the climate signal is imprinted in the snow (e. g. Casado et al., 2016; Freitag et al., 2013b; Hörhold et al., 2012; Laepple et al., 2017; Münch et al., 2017). This study aims at a better understanding of the spatial and temporal variability of stable isotopes in a specific study site on the Antarctic continent.

1.1. Background and motivation

The Antarctic continent covers about 8.3 % of the global land surface and plays a key role in the Earth's climate system (IPCC, 2013). However, the amount of available data from this region combining observation and proxy data is very low.

Jones et al. (2016) assessed in their comprehensive study the temperature variability in the high-latitude Southern Hemisphere for the last 200 years. They overcome the sparsely spatial distribution of instrumental records by comparing and analysing information from several record types (Figure 1.1).

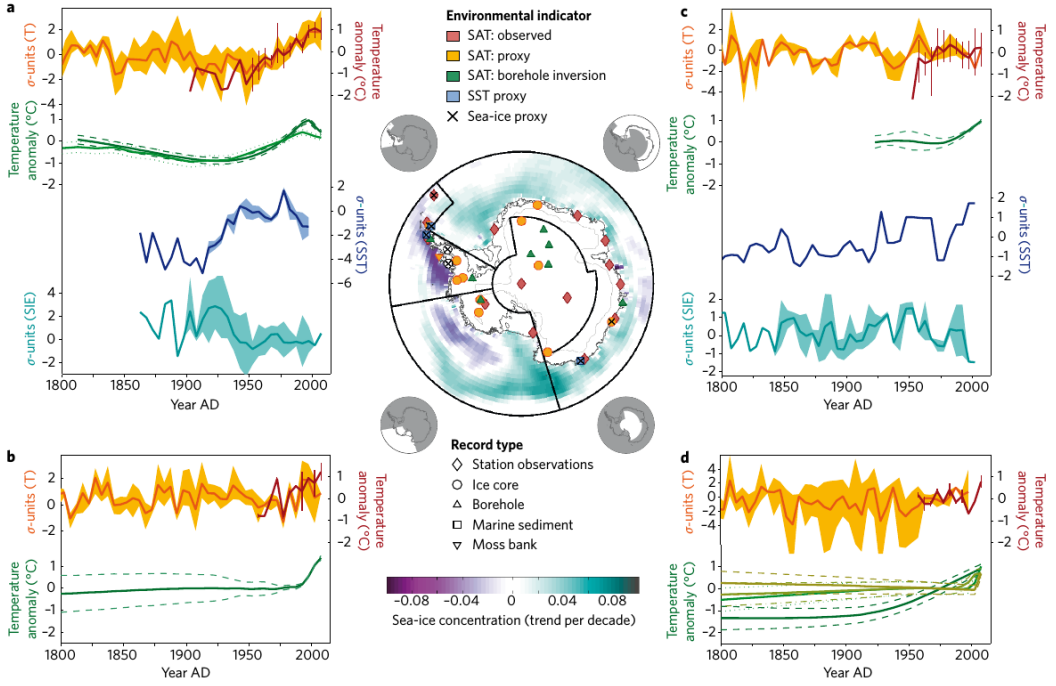

Figure 1.1.: Assessment of temperature variability and trends on the Antarctic continent for the past 200 years displayed by instrumental, satellite, proxy and reanalysis data (Jones et al., 2016, Fig. 2). The study areas are separated into a) the Antarctic Peninsula, b) West Antarctica, c) coastal East Antarctica and d) the Antarctic Plateau (indicated by black lines in the map). All data show either temperature anomalies relative to the period 1960 - 1990 (°C units) or normalized data (σ-units), thick lines are 5-year averages. The type (symbol), the associated environmental indication (colour) and the geographic location of each record is shown. Shading of the ocean indicates the decadal trend in sea-ice concentration for the period from 1979 to 2014. SAT: surface air temperature; SST: surface sea temperature.

The uncertainty for reconstructed temperature anomalies (deviation from the mean relative to 1960 - 1990, Figure 1.1 orange lines) are relatively low for the Antarctic Peninsula, West Antarctica and coastal East Antarctica during the last two centuries. Furthermore, all borehole measurements indicate a temperature increase towards the end of the 20$^{\text{th}}$ (Figure 1.1 green lines). Additionally, a further study from Steig et al. (2009) reveals a significant continent-wide warming based on surface temperatures derived from satellite thermal infrared measurements combined with data from automatic weather stations (AWS) for the time period from 1957 to 2006. For eastern Antarctica the trend amounts to $0.10\,^{\circ}\text{C} \pm 0.07\,^{\circ}\text{C}$ per decade. In contrast to these findings, the results by Jones et al. (2016) show for the Antarctic Plateau (AP) (Figure 1.1, region d)) shows no increasing temperatures during the 20$^{\text{th}}$ century. However, the uncertainties of the reconstruction are high hampering a meaningful estimation of recent trends and further providing the mo-

tivation to study potential site specific temperature trends during the last 50 years in this region.

Measured isotopic compositions from precipitation and snowfall on the AP differ strongly from surface snow samples (Casado et al., 2016). This means that other, non-climatic effects alter the isotopic composition after the deposition. Thus, the initial temperature signal which is assumed to be apparent in the precipitation is not completely preserved (Casado et al., 2016; Münch et al., 2016).

Wind and surface roughness cause irregular deposition of snow leading to a non-climatic effect on small scales which is known as stratigraphic noise (Fisher et al., 1985). Moreover, inter-annual variations of isotopic compositions are driven by precipitation intermittency and varying seasonal precipitation events (Richardson-Näslund, 2004). Additionally, post-depositional modifications occurring directly at or close to the snow surface are thought to cause further alterations in the isotopic composition (Münch et al., 2017). It is therefore important to determine the non-climatic contribution to reliably interpret stable water isotopologues from ice cores (Masson-Delmotte et al., 2008; Schneider and Steig, 2008).

The motivation to average several cores in order to minimize the amount of noise is based on the above presented discrepancies between isotopic signals and local temperatures. Hence, averaging allows an improved signal-to-noise ratio and provides the possibility to better assess the question of a temperature trend on the AP (Münch et al., 2016). Based on the presented information and previous studies on climate variability on the Antarctic continent, a study site in Dronning Maud Land (DML) on the AP was chosen to investigate spatial and temporal variability of stable isotopes in water. Therefore eleven firn cores are measured and analysed together with already existing data from firn cores, snow pits and trenches. Comparisons of different sampling, measuring and post-run correction methods are conducted to determine possible discrepancies caused by these. Moreover, the new gained firn profiles are stacked to one data set reducing the noise while emphasizing the climate signal. Temporal variability and trends during the last two centuries are discussed.

1.2. Outline of this study

A detailed structure of this thesis is given in the following:

Chapter 2 provides a theoretical introduction to stable water isotopologues. Furthermore, important processes between snow accumulation and the transformation to ice are explained.

In the beginning of Chapter 3 the study site is presented. Then, several sampling and measuring methods are explained followed by a discussion of the different post-run correction techniques to process the raw data. Afterwards, the dating procedure, all used data and all steps which are needed to create the stack from the single profiles are presented.

Chapter 4 presents the main results of this thesis. First, a comparison between different sampling, measuring and correction procedures is shown which addresses

the questions whether different methods cause significant deviations in the data. Secondly, mean annual accumulation rates are derived and analysed and the spatial and temporal variability of stable isotopes in water is addressed. Finally, the stacked record is illustrated, the variability between several profiles as well as the temporal trend during the last 200 years are discussed and the paleoclimatic significance of the derived data set with regard to the general global warming trend is discussed.

Chapter 5 summarises the main results of this thesis and provides an outlook for possible future analyses.

2. Introduction to isotopes, polar snow and firn

This chapter gives a theoretical overview on stable isotopes in water molecules, their natural occurrence and the relation to temperature. Afterwards, the development of the firn column is illustrated by explaining the individual contributions from accumulation, densification and diffusion.

2.1. Isotopic composition of water

Oxygen has three naturally occurring isotopes of which ^{16}O is the lightest and most abundant isotope while ^{17}O and ^{18}O occur less frequently. Hydrogen has two naturally occurring isotopes: ^{1}H and ^{2}H (also known as deuterium D). The most common isotopologues of water are therefore H_2O^{16}, HDO^{16} and H_2O^{18} (Dansgaard, 1964) which differ in their physical behaviour during phase transitions. The volatility of the light molecule H_2O^{16} is higher than for the heavier molecules which leads to fractionation during evaporation and condensation.

The amount of fractionation can be quantified using the fractionation factor α which is temperature dependent. This factor expresses the difference in vapor pressures between the light and the heavy molecules and is relevant in two processes, both assume a slow fractionation. The first process describes a closed system in which an equilibrium between the liquid phase and the condensate can establish. In particular, α describes here the ratio between the vapour pressure of the light component (p) and the heavy component (p'):

$$\alpha = \frac{p}{p'} \ . \tag{2.1}$$

The second process, denoted as a Rayleigh process, represents the fractionation in an open system in which the condensate is removed immediately after the formation and thus leads to higher fractionation rates (Dansgaard, 1964). In a Rayleigh process, the isotopic ratio R (e. g. H_2O^{18}/H_2O^{16}) of the remaining phase changes according to

$$R = R_0 f^{\alpha - 1} \tag{2.2}$$

where R_0 describes the initial isotopic ratio and f the remaining fraction of the initial phase.

Condensation processes in clouds are approximated to happen under Rayleigh conditions. It is assumed that Rayleigh fractionation, apart from additional fractionation due to kinetic effects under supersaturated conditions, is the driving factor

for the varying isotopologue composition observed in snow, firn and ice (Jouzel and Merlivat, 1984). Thus, the falling snow is enriched in the heavier isotopologues while the remaining water vapor in the cloud is enriched in the lighter ones. Towards higher altitudes and continental regions the precipitation is increasingly depleted in the heavy isotopes D and ^{18}O due to successive stages of precipitation formation. The air cools more and more and experiences isotopic depletion. Hence, the isotope content in precipitation varies with and is dependent on changing temperatures.

The δ-notation is commonly used to express the ratio of heavy to light isotopes (for oxygen e. g. $^{18}O/^{16}O$ and for hydrogen D/H) in a sample relative to a reference:

$$\delta = \left(\frac{R_{\text{sample}}}{R_{\text{reference}}} - 1 \right) \cdot 10^3 \quad [‰] \tag{2.3}$$

(Craig, 1961; Dansgaard, 1964). The common reference water is defined by the international VSMOW/SLAP scale. VSMOW (Vienna Standard Mean Ocean Water) is fixed to 0 ‰ for both oxygen and hydrogen isotopes and the reference water SLAP (Standard Light Antarctic Precipitation) is -55.5 ‰ for $\delta^{18}O$ and -428 ‰ for δD relative to VSMOW (Gonfiantini, 1978).

Based on the presented fractionation between heavy and light water molecules, an almost linear relation between hydrogen and oxygen isotopes exists (Craig, 1961):

$$\delta D \approx 8 \times \delta^{18}O + 10 \quad [‰] \; . \tag{2.4}$$

Consequently, measured hydrogen and oxygen isotopes generally reveal similar information on e. g. derived temperature changes.

The deviation from the linear relationship between $\delta^{18}O$ and δD (Eq. 2.4) can be described using the second order parameter deuterium excess (d.excess) which is defined as

$$\text{d.excess} = \delta D - 8 \times \delta^{18}O \quad [‰] \tag{2.5}$$

(Dansgaard, 1964). Kinetic effects during evaporation lead to deviations from the above mentioned parallelism (Dansgaard, 1964). Thus, d.excess reveals information on small scale processes (e. g. distillation) at the source and deposition site (e. g. Touzeau et al., 2016; Vimeux et al., 2001).

2.2. Polar firn and ice and its isotopic composition

Accumulated snow on an ice sheet compacts during time due to the weight of the overlying snow resulting in increasing densities with depth. Furthermore, diffusion alters the isotopic signals in the snow cover. The following subsections illustrate the hydrological cycle of water from the evaporative source to the deposition and describe the processes of accumulation, densification and diffusion in more detail.

Isotopic composition of polar snow and firn

The isotopic composition of snow and ice differs greatly over the entire Antarctic continent. For a given site the isotopic ratios are strongly dependent on the altitude and the mean annual temperature. Figure 2.1 illustrates the hydrological cycle from the evaporative source in the ocean to the deposition on a polar ice sheet and corresponding exemplary ratios for the stable oxygen isotope ^{18}O. Rayleigh distillation determines the isotopic composition of falling snow during water vapor condensation in a cloud over the entire AP, leading to decreasing isotopic ratios at higher elevations and colder regions (Dansgaard, 1964). However, temperature is not the only factor influencing the isotopic variability. In the following, several additional contributions will be discussed.

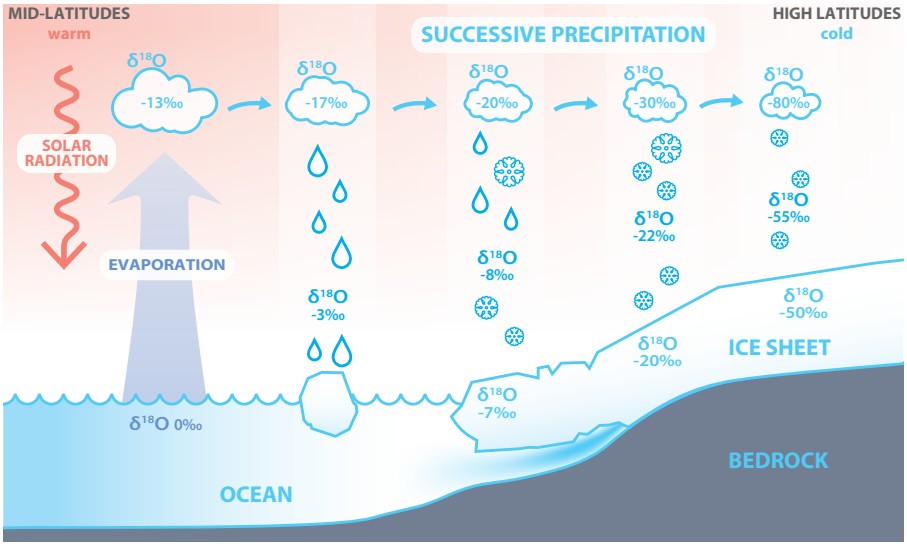

Figure 2.1.: Illustration of the hydrological cycle from the evaporative source in the ocean to the deposition on the Antarctic ice sheet. Decreasing isotopic ratios are due to fractionation in successive precipitation events during which heavy isotopologues precipitate preferentially, leaving the remaining water vapour enriched in light isotopologues. Image by Mathieu Casado.

Accumulation

The total amount of annual accumulation on the Antarctic continent is site-specific and depends on meteorological (e. g. annual mean temperature) and geographic conditions (i. e. elevation and continentality) (Fujita et al., 2011; Richardson-Näslund, 2004). Snowfall occurs highly episodically over the year. Approximately eight high-precipitation events account for more than half of the total annual accumulation in DML (Schlosser et al., 2010). Furthermore, accumulation patterns are complex and show large spatial variations, mainly caused by wind-driven redistribution, sastrugi formation and short-term climatic variations. Additionally, the ice sheet surface slope, surface topography and bedrock topography cause local variations as well (Fujita et al., 2011; Richardson et al., 1997; Richardson-Näslund, 2004).

Measurements of present-day accumulation rates are possible (e. g. at AWSs), albeit the quantification of the intermittency and the seasonal variations during a

year remains difficult (Freitag et al., 2013a; Hörhold et al., 2012; Laepple et al., 2016). In summary, the analysis of ice cores can reveal past annual accumulation rates, however, variations throughout a year are difficult to retrieve.

Densification and diffusion

Loose snow and firn is a porous medium consisting of a mixture of ice grains and open pore spaces filled with air. Due to the increasing weight of the overlying snow with increasing depth, the snow compacts and the density increases (Figure 2.2). The process of firn densification can be separated into several stages (Herron and Langway, 1980). The transition from densities of 300 to 400 $\mathrm{kg\,m^{-3}}$ at the surface to densities of $\sim 550\,\mathrm{kg\,m^{-3}}$ describes the change from loose snow to firn which happens relatively fast. Further densification occurs comparatively slow. Higher densities involve lower porosity, lower sublimation and increasing contact between individual grains. Important processes are grain settling and packing.

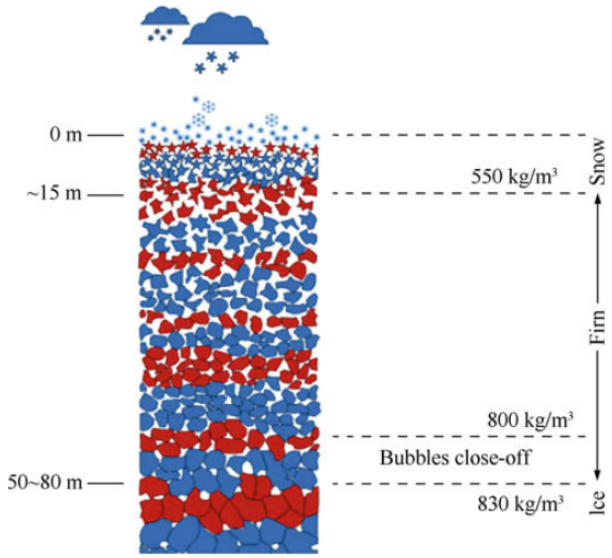

Figure 2.2.: Schematic illustration of snow densification from loose snow via firn to ice (Talalay, 2016, Fig. 1.8). The transition depths from snow to firn and from firn to ice are defined by specific densities, total depths vary depending on mean annual temperatures and accumulation rates.

After the transition from snow to firn, compaction continues with decreasing pore spaces until the 'close-off' zone at a density between 800 and 830 $\mathrm{kg\,m^{-3}}$. Below this depth no exchange of air between pores is possible. Recrystallization, deformation and molecular diffusion alter the shape and size of ice crystals and lead to the formation of ice (Fujita et al., 2009; Maeno and Ebinuma, 1983).

The depths of the snow-to-firn- and the firn-to-ice-transition depend mainly on the mean annual temperature (Nishimura et al., 1983). The latter one is typically found in depths of 50 to 80 m (Figure 2.2) corresponding to ages of 100 to 300 years. Figure 2.3 shows depth-density profiles for different climatic regions. Vostok (78.5 °S, 106.8 °E) exhibits the lowest densification rate due to cold and dry conditions (Cuffey and Paterson, 2010). The transition from firn to ice occurs here in a depth of 95 m

after 2,500 years while at Byrd (80.02 °S, 119.53 °W) the transition is in 64 m after 280 years (Cuffey and Paterson, 2010).

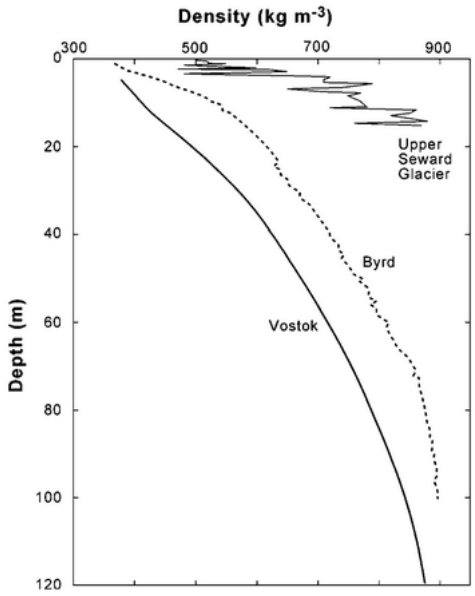

Figure 2.3.: Depth-density profiles from ice cores from a glacier in Canada (Upper Seward glacier), in West Antarctica (Byrd) and in East Antarctica (Vostok). The last two are smoothed. The annual temperature at Vostok is -57 °C and -28 °C at Byrd with mean annual accumulation rates of 22 mm water equivalent per year (mm w. eq. yr^{-1}) and 140 mm w. eq. yr^{-1}, respectively (Cuffey and Paterson, 2010, Fig. 2.3 and references therein).

Herron and Langway (1980) made use of the dominant role of the temperature parameter to develop a firn densification model (herafter referred to HL model). As a function of mean annual temperature, mean annual accumulation rate and initial snow density at the surface, the HL model yields depth-density and depth-age relations. Constantly spaced samples (e. g. at a resolution of 10 cm) contain less temporal information at the surface than at a greater depth. Hence, firn densification is an important process to consider when comparing data from different depth intervals.

Not only the density of snow is altered after the deposition, but also the initial isotopic composition is changed due to isotopic diffusion (Whillans and Grootes, 1985). The seasonal stratigraphy is most affected by the diffusional smoothing while decadal and longer-term signals remain, depending on the local accumulation rate and the ambient temperature. The diffusional smoothing of isotopic records is primarily driven by vertical gradients in the isotopic composition. Diffusion happens much faster in firn and much slower in ice due to the higher densities in firn and ice at greater depths (Cuffey and Steig, 1998; Johnsen et al., 2000; Whillans and Grootes, 1985).

3. Methods and data

This chapter presents the study site and then focuses on the variety of sampling methods for snow and firn as well as measuring methods for stable water isotopologues and associated post-run corrections. Furthermore, different ways of establishing a depth-age conversion are described and the analysed data sets are presented. In the end, the procedure of building a stack from several profiles in order to improve the signal-to-noise ratio is illustrated.

3.1. Study site

The study sites for all analysed data are located around the Kohnen research station in DML (Figure 3.1, red box) on the AP. The respective part of the plateau lies in the Atlantic Sector on the Antarctic continent. Hence, precipitation and snow fall have their moisture origin in the Atlantic Ocean. The distance from the Kohnen station to the nearest coast is approximately 400 km.

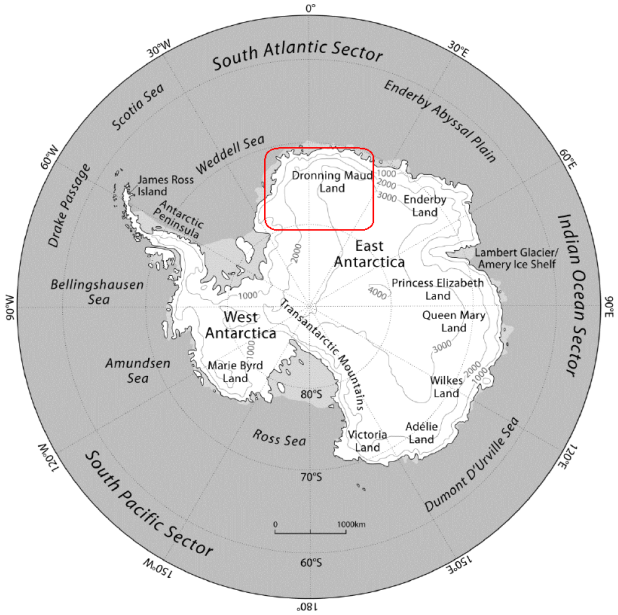

Figure 3.1.: Map of the Antarctic continent showing the area of investigation in Dronning Maud Land (red box) on the Antarctic Plateau (Jones et al., 2016, supplementary material Fig. 1, modified).

The Institute for Marine and Atmospheric Research from Utrecht University installed an automatic weather station (AWS 9, 75 °S, 0 °E, ~2900 m a.s.l.) in December 1997 in this region. Temperature, humidity, wind speed and wind direction, incoming and outgoing radiation, snow height as well as snow temperatures are constantly measured (Reijmer, 2001).

The Kohnen research station was established in the austral summer seasons 1999 to 2001 during the pre-site survey for the international drilling program EPICA (European Project for Ice Coring in Antarctica) and is situated in the immediate vicinity to the AWS 9. The total length of the EPICA ice core which was drilled between 2002 and 2006 is 3,190 m and thus provides information on climatic conditions over the last 150,000 years (EPICA community members, 2006). This region in DML is characterised by low mean annual accumulation rates of about 61 mm water equivalent per year (mm w.eq. yr^{-1}) (Oerter et al., 1999) which provides the possibility to reconstruct climatic timeseries over a long period of time. The low ice flow of 2 m yr^{-1} ensures that the measured signal was recorded in the same area (Drücker et al., 2002). Table 3.1 summarizes geographic and meteorological information on the EPICA drilling site. The main wind direction is from northeast to east (corresponding to 65° from geographic north) (Reijmer and van den Broeke, 2003).

Table 3.1.: Information on the EPICA drilling site in DML. Geographic location, 10 m firn temperature (T_{firn}), mean annual accumulation rates (acc rate) and mean daily wind speed (v_{wind}) are presented.

Latitude °N	Longitude °E	Elevation (m a.s.l.)	T_{firn} (°C)	acc rate (mm w.eq. yr^{-1})	v_{wind} ($m\,s^{-1}$)
-75.0[1]	0.1[1]	2892[1]	-44.5[1]	61	4.4 ± 2.3[3]

[1] EPICA community members (2006), [2] Oerter et al. (1999), [3] v_{wind} ±1 standard deviation from AWS 9 for the period 1998 - 2013 (Reijmer and van den Broeke, 2003)

Falling snow is not evenly distributed over the Antarctic continent. In general, mean annual accumulation rates decrease from the coast towards the interior of the continent (Casado et al., 2016). Furthermore, the isotopic composition of the ice sheet in DML is determined by the mean annual temperature as explained in Chapter 2. Hatvani et al. (2017) simulated the spatial distribution of mean $\delta^{18}O$ values for the period from 1970 to 1988 for eastern parts of the AP (Figure 3.2). The effect of decreasing isotopic ratios with rising elevation and increasing distance to the coast is evident. For the study area in this thesis, isotopic ratios from -40 to -50 ‰ are therefore expected and in good agreement with previously measured values (e. g. Oerter et al., 1999).

3.2. Sampling and measuring methods

This study is based on the analysis of different types of samples from firn cores, snow pits and snow trenches from DML which have been measured according to different methods. Varying post-run correction schemes have been applied. In the following all used sample types as well as measuring and calibration schemes are presented.

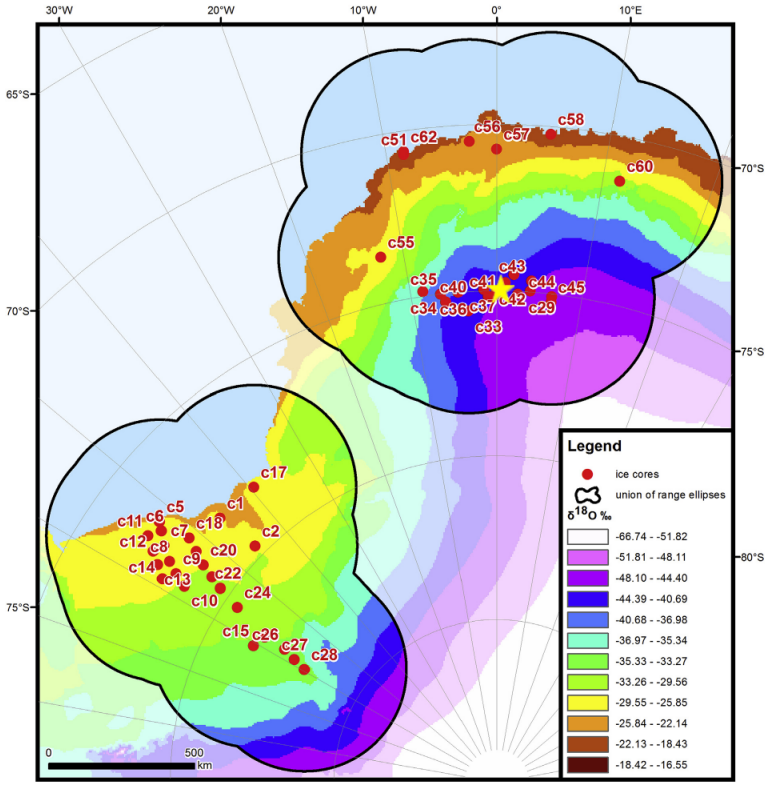

Figure 3.2.: Illustration of modeled mean δ^{18}O values for the time period 1970 to 1988 for parts of the Atlantic Sector in East Antarctica: Filchner-Ronne-, Riiser-Larsen- and Fimbul-ice shelves (Hatvani et al., 2017, Fig. 5, modified). The yellow star indicates the position of the Kohnen research station.

Sampling in the field

The analysis of samples from firn or ice cores yield information on the long-term climatic history of this specific location. Firn cores are drilled with special firn core drill heads which differ from drill heads for ice (Talalay, 2016). In the following, the drilling procedure is described as it is performed at the Alfred Wegener Institute for Polar and Marine Research (AWI). A typical drilling construction is illustrated in Figure 3.3 (a). After drilling, the obtained firn or ice is cut and sorted into 1-meter segments (0.00 - 0.99 m, 1.00 - 1.99 m, etc.). Diameter and weight of each segment are noted. In the upper meter of the core, deviations from the normal diameter of 98 mm are possible due to the higher porosity. Afterwards, each 1-meter segment is packed in a polyethylene bag. Six meters are always put together in a polystyrene box and are stored preferably below -20 °C. After shipping the boxes to the AWI in Bremerhaven, Germany, the segments have to be prepared in order to measure the desired parameters (e. g. δ^{18}O). A small amount of sample is sufficient for discrete isotope measurements, hence horizontally five to seven centimeters are enough to achieve the required amount of sample (Figure 3.4). For continuous measurements a rod with a $\sim 3 \times \sim 3$ cm cross section is necessary. In order to prepare the core adequately, AWI operates a horizontal bandsaw in an ice laboratory (Figure 3.5).

While ice cores yield information on long timescales with a coarse resolution, snow pits allow studies on short timescales at high temporal resolutions. For this,

(a)

(b)

Figure 3.3.: Different approaches to sample snow and ice: (a) drilling (firn or) ice cores (Talalay, 2016, Fig. 9.70), (b) snow trenches (T. Laepple).

vertical profiles are generally sampled in a resolution of some centimeters. Snow pits are therefore a comparatively fast and simple way to gain samples. In addition to snow samples, information on physical properties (e. g. density and temperature) are measured in the field as well.

Snow trenches (Figure 3.3 (b)) present a vertical snow profile with a horizontal extension and enable the sampling of horizontal layers. Samples are taken in predefined horizontal and vertical intervals (Münch et al., 2016, 2017). Samples from snow pits and trenches are packed individually in small and sealed polyethylene bags and kept frozen until the measurement. Snow trenches, or several snow pits close to each other, are a useful tool to study the horizontal variability in isotopic compositions and physical snow properties (e. g. density) (Laepple et al., 2016; Münch et al., 2016).

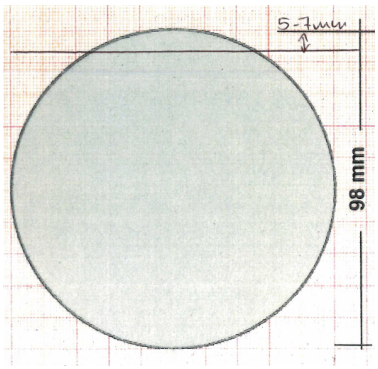

Figure 3.4.: Cutting plan for firn cores.

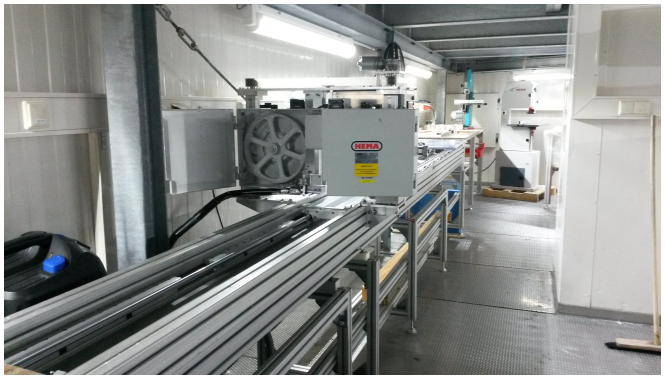

Figure 3.5.: Bandsaw in the ice laboratory (-20 °C) at the AWI in Bremerhaven.

Measurement of stable isotopes in water

Ratios of stable isotopes in water ($^{18}O/^{16}O$ and D/H) from discrete snow samples can be measured using traditional Isotope Ratio Mass Spectrometers (IRMS) or more modern Cavity Ring-Down Spectrometers (CRDS). The IRMS method is based on differences in mass numbers of the respective element and delivers reliable

results with low uncertainties. Nevertheless, high operational costs, time-consuming preparation and the need of large amounts of samples led to an increased application of near-infrared spectrometers, the CRDS method, which measures isotopic ratios based on differences in characteristic electromagnetic wave absorption at specific wavelengths (Kerstel et al., 1999). Cavity ring-down instruments are commercially produced by e. g. Picarro Inc. (Picarro Inc., 2018).

For the CRDS method, melted ice samples are filled in glas vials and placed at a pre-defined position in a measuring rack. From each vial, a syringe extracts a specific amount of sample and injects it into the measurement device (Figure 3.6). Then, the injected sample is completely vaporized inside the instrument and directed into a cavity. Once the laser is turned on, the cavity fills with circulating light. Then, the laser is switched off and the 'ring-down' time, the time it takes until the cavity is empty again, is measured. Since the ring-down time is different for different isotopologues of the water molecule, the instrument is able to determine the isotopic abundance in the sample (Figure 3.7).

The achieved precision is typically higher than 0.1 ‰ for $\delta^{18}O$ and 0.5 ‰ for δD measurements (Kerstel and Gianfrani, 2008) which is in the magnitude of the precision of IRMS instruments. The CRDS technique and therefore resulting raw data from e. g. Picarro instruments show memory- and drift-effects and require a final calibration to international standards (Piarro Inc., 2018). Different post-run correction schemes are presented in the end of this section.

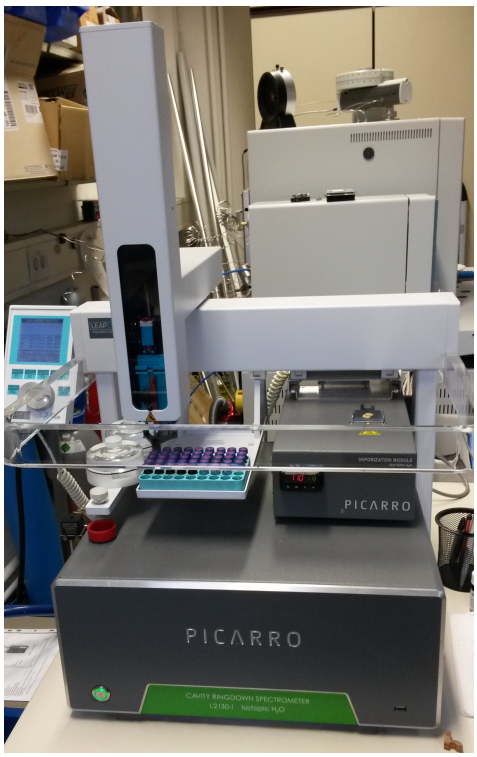

Figure 3.6.: Cavity-Ring Down Spectroscopy instrument (L2130-i, Picarro Inc.) operated in the isotope laboratory of the Alfred Wegener Institute in Potsdam, Germany.

In addition to the discrete sampling and measuring method, the Continuous Flow

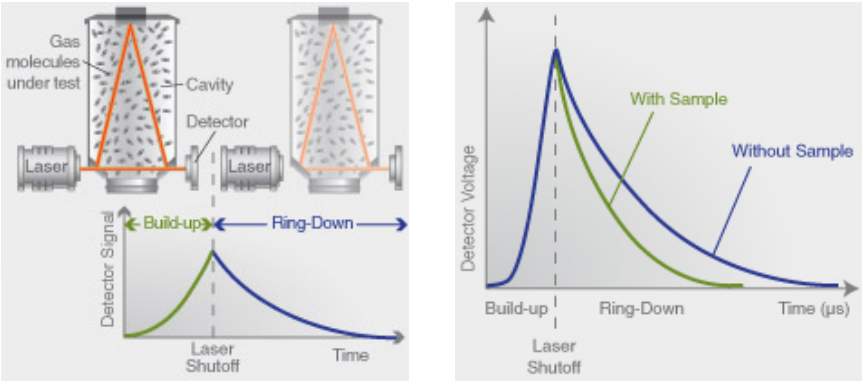

(a) (b)

Figure 3.7.: Schematic illustration of the operating principle of a Picarro CRDS analyzer. (a) Setup of the measurement module, (b) Light intensity as a function of measurement time with and without sample gas in the cavity (Piarro Inc., 2018).

Analysis (CFA) system presents a further way to sample and measure isotopic ratios in firn or ice cores associated with a high depth resolution (Kaufmann et al., 2008). Entire core segments of up to one meter length can be measured in a comparatively short duration. However, it is not applicable for discrete samples from snow pits and trenches.

A CFA system consists of a melting unit, a distribution unit and an analysis unit (Figure 3.8). The melting unit ensures a constant sampling rate through a steady melt process. A prepared ice or firn core (cross section of $\sim 3 \times \sim 3\,\mathrm{cm}$) stands vertically on the melter head surrounded by a plexiglas box in a cold room (-16 to -20 °C) (McConnell et al., 2002). The resulting water flow is separated in the distribution unit leading to several measuring modules, e. g. to a CRDS instrument which directly measures the isotopic composition. The melting rate depends on the density of the core. In order to prevent the melt water to blur, the speed of the melt process is lower in firn which leads to a higher resolution of $\sim 1\,\mathrm{cm}$ in ice than in firn ($\sim 2\,\mathrm{cm}$). Additionally to the CRDS instrument, further devices can be attached to the distribution unit measuring chemical parameters or impurities (e. g. Ca^{2+}, Na^{+} or $NH_4{}^{+}$).

Discrete sampling is more labor-intensive for firn and ice cores and requires more sample preparation compared to the use of a CFA system which melts one meter of ice in approximately 30 minutes, depending on the melting rate and the porosity of the core. However, discrete high resolution measurements provide more accurate values for minima and maxima in $\delta^{18}O$ and δD data because the steady melt process leads to indistinct peaks (Kirstin Hoffmann, personal communication). A detailed comparison for data from both, discrete and continuous methods, is presented in Chapter 4.1.

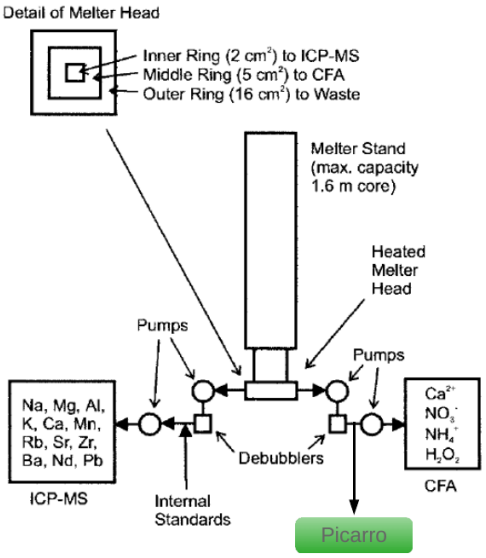

Figure 3.8.: Schematic illustration of a setup for a CFA system with an attached CRDS device (McConnell et al., 2002, Fig. 1 modified).

Post-run correction for CRDS data

Raw data from a discrete measurement with a CRDS instrument require a post-run correction for analytical effects (as memory and drift) and subsequent calibration to international reference materials (Piarro Inc., 2018; van Geldern and Barth, 2012). All presented equations in the following are based on the post-run correction procedure presented in van Geldern and Barth (2012). In order to scale and normalize raw data, reference waters with known isotopic ratios are analysed in three blocks throughout the measurement sequence; in the beginning, in the middle part and in the end.

A syringe takes a specific amount of water from each vial and injects it into the spectrometer, where the sample is vaporized and measured as explained above. A memory-effect which arises from the carry-over of residual amounts of vapor of the previous sample in the measurement cell (van Geldern and Barth, 2012). Thus, one single injection is always affected by the previous one. After several injections from the same vial, the measured value comes very close to the true value; thus, multiple injections from each vial are conducted. A memory coefficient m can be calculated as

$$m_i^n = \frac{\delta_t^{(n-1)} - \delta_i^n}{\delta_t^{(n-1)} - \delta_t^n} \tag{3.1}$$

where n denotes the sample position in the rack and i the number of the injection. δ_t^n indicates the value considered as the real value for the current sample and $\delta_t^{(n-1)}$ of the preceding sample. The measured result reaches a stable value δ_t typically after five injections for δ^{18}O and eight injections for δD measurements (van Geldern and Barth, 2012). Once the memory coefficients are determined, the memory-corrected

isotopic ratio for all following samples can be calculated according to

$$\delta_{\text{memory corrected}} = \delta^{n}_{i\ (\text{raw})} + (1 - m_i) \times \left(\delta^{n}_{i\ (\text{raw})} - \delta^{(n-1)}_{t}\right) . \tag{3.2}$$

Furthermore, reference waters measured in the beginning and in the end of a measurement sequence can exhibit an analytical drift throughout the measurement. The comparison of all reference waters during the run allows the quantification of this drift which is time-dependent and in general very small (over 24 hours < 0.2 ‰ for δ^{18}O and < 1‰ for δD) (van Geldern and Barth, 2012). Drift-corrected values are calculated using the estimated linear drift slope ds and the number n of the vial in the sequence which is proportional to the measurement time:

$$\delta_{\text{drift corrected}} = \delta_{\text{memory corrected}} + (ds \times n) . \tag{3.3}$$

After memory- and drift-correction, data have to be normalized to the international VSMOW scale (Gonfiantini, 1978). A linear regression is calculated using the known in-house reference waters from the first and the last standard block. Slope α and intercept β are used to scale the measured values as

$$\delta_{\text{final}} = \alpha \times \delta_{\text{drift corrected}} + \beta . \tag{3.4}$$

For the illustrated post-run correction different schemes are available of which three are presented in the following. The first procedure is based on the presented study from van Geldern and Barth (2012) using an Excel-sheet based method (hereafter referred to as 'EvG'). The in-house reference waters in the first block are injected ten times and four injections are conducted for all further samples and reference waters. The measurement time for 33 samples plus the reference waters is about 29 hours.

A second processing scheme exists using likewise Excel, but with modifications in the number and the use of the injections (abbreviated as 'E6Inj'). From each vial, regardless of the content, six injections are performed. The first block contains two vials for each reference water, resulting in 12 injections per standard. Unlike the EvG method, only the last three injections of each vial are used for deriving the memory coefficient and calculating the processed data. The increased number of injections lead to a measurement time of about 48 hours for 33 samples.

The third correction scheme requires the statistical software R (R Core Team, 2017) and the package 'piccr' (Münch, 2017) (referred to as 'piccr' in the following). The first block of reference waters is structured in the same way as in the 'E6Inj' method. However, all following samples and standards are only injected three times. Hence, the measurement time decreases notably to about 25 hours for 33 samples. Small differences in the algorithm for the drift-correction exist between this method and Eq. 3.3 from van Geldern and Barth (2012). The Excel-based scheme considers only a potential drift of the calibration intercept while the 'piccr' package can correct for a potential drift of the calibration slope (Thomas Münch, personal com-

munication). However, the differing methods only have a minor influence on the corrected data.

Previously measured and analysed data are mostly processed with the post-run correction schemes EvG and E6Inj. For all raw data calibrations of newly obtained data for this thesis, 'piccr' was applied. A detailed comparison between these three correction schemes is presented in Section 4.1.

3.3. Dating

Densification processes throughout the ice sheet, as explained in chapter 2.2, lead to a nonlinear relationship between the absolute depth and the temporal scale. Therefore, a depth-age-conversion is necessary. There are two widely used methods for this: (1) annual layer counting and (2) the use of volcanic horizons as time markers. Prior to this, a conversion from true logging depth to depth in water equivalent is necessary to account for the compaction and thinning of the firn and ice layers (Hörhold et al., 2011). This conversion as well as both dating methods are presented in the following.

Depth in water equivalent (w. eq.) expresses the amount of water included in the respective amount of snow, firn or ice allowing direct comparisons of different depth intervals. The water equivalent depth $z_{w.eq.}$ is calculated using the equation

$$z_{w.eq.n} = z_{log_{n-1}} + (z_{log_n} - z_{log_{n-1}}) \cdot \rho_n \tag{3.5}$$

with n being the number of the respective depth interval of the logging depth z_{log}. ρ_n describes the density ratio between the density of the firn segment and the density of water. High quality and high resolution density measurements in porous firn cores are difficult. However, an X-ray microfocus computer tomograph was developed at the AWI in Bremerhaven especially designed for porous firn cores (Freitag et al., 2013a). In the case of no available density data, for this thesis density values are simulated using the HL model (see Section 2.1). Required initial surface densities can be estimated depending on the particular study site.

For the method of counting annual layers, measured impurity concentrations (e. g. in a CFA system) are used. Peaks in impurity concentrations (e. g. Ca^{2+}, Na^+ or $NH_4{}^+$) can be ascribed to the winter season marking the end of a year, hence annular layers can be counted (Freitag et al., 2013b). Electrical properties in Dielectric Profiling (DEP) data also show annual peaks caused by higher ion concentrations during the summer season. Thus, on the basis of either impurity concentrations or DEP data annual layers can be detected and counted. When analysing several cores, common horizons of volcanic ash layers are additionally used to match the profiles among each other (Oerter et al., 2000).

A depth-age conversion is also possible for ice cores without impurity measurements using only volcanic layers which are defined by increased acidity and/or an increased concentration of H_2SO_4 leading to peaks in conductivity data. Peaks are generally characterised by a short duration and often have a symmetrical shape(Karlöf et al., 2000). Hence, the depths of large peaks can be ascribed to prominent volcanic

eruptions and a temporal scale is linearly interpolated in between. Moreover, these layers can serve as match points to synchronize several cores. If a peak is not clearly identifiable, a comparison of the shape of the conductivity profile in the expected depth interval with profiles from neighboring cores can help to determine a layer. This dating procedure has been applied in studies for Antarctic and Greenlandic cores and reveals reliable chronologies (Karlöf et al., 2000; Weißbach et al., 2016).

For this thesis, dating has been performed based on the simple linear interpolation between known volcanic layers. However, in general the count of annual layers is more precise than the linear interpolation between volcanic ash layers. The dating uncertainty of this simple approach can therefore be estimated by comparing an annual layer counted chronology to the simple depth-age conversion from the same core.

3.4. Data

In this thesis, several firn cores drilled in different seasons as well as data from snow pits and snow trenches are analysed to assess the spatial and temporal variability of stable water isotopologues in DML on the AP. In the following section all used data, their locations, obtained resolutions, used sampling and measuring methods as well as used post-run correction schemes are described. The available data divides into previously measured and (partly) published data as well as new data obtained for this thesis.

Previously measured and analysed data

Table 3.2 gives an overview about the type of samples, the respective locations, the sampling or drilling dates and measuring and correction methods for all previously analysed data which are also part of this thesis.

The firn cores B31, B32 and B33 were drilled in the austral summer season 1997/98 and cover more than the last 1,000 years BP. Results from isotopic analyses are published in Oerter et al. (1999) and Graf et al. (2002). The vertical resolution is ~10 cm; isotope ratios were measured in a traditional mass spectrometer. All cores have been dated by annual layer counting. The drilling location for B31 lies at the lowest elevation (2,669 m a.s.l.) of all analysed cores, the location of B33 is at the highest elevation (3,160 m a.s.l.) (Sommer et al., 2000), corresponding to a maximum difference in elevation of 491 m. Geographic locations for B31, B32 and B33 are indicated in blue in Figure 3.9, distances between all sites are listed in Table C.1 in the Appendix.

Furthermore, five firn cores drilled in the austral summer season 2012/13 are likewise analysed. These lie close to the Kohnen research station in DML and are indicated in green in Figure 3.9. Isotopic ratios for B40 were measured in a CFA system at the Desert Research Institute in Reno, USA, at a vertical resolution of 1 cm. Firn cores B41, B42, B49 and B50 were measured discretely at a resolution of 2 cm with a CRDS instrument at the AWI Bremerhaven using the correction scheme EvG.

So far, no dating has been performed (Maria Hörhold, personal communication).

In addition to already existing long-term data from firn cores, available data from snow pits and snow trenches are also subject of this study. The snow pits KOH1 to KOH8 cover the upper 25 cm of snow. The upper 3 cm were measured at a resolution of 0.5 cm followed by a resolution of 1 cm. The distribution of sampling locations for all snow pits as well as for the snow trenches is indicated in dark blue and red, respectively, in Figure 3.9. Snow pit KOH1 lies on the southern site of Kohnen, while KOH2 to KOH8 form a straight line towards northeast. All snow pits were measured with a Picarro device and corrected with the EvG scheme. Snow trenches T15-1 and T15-2 were sampled in the season 2014/15. The sampled depth is 3.4 m with a vertical resolution of 3 cm for depths up to approximately 2.4 m and of about 2.2 cm below. In each trench, eleven profiles were sampled at a horizontal spacing of 5 m. The horizontal distance between the starting points of the snow trenches is 550 m. All discrete samples from the trenches were measured with Picarro instruments at AWI Potsdam and corrected with the piccr scheme (Münch et al., 2017).

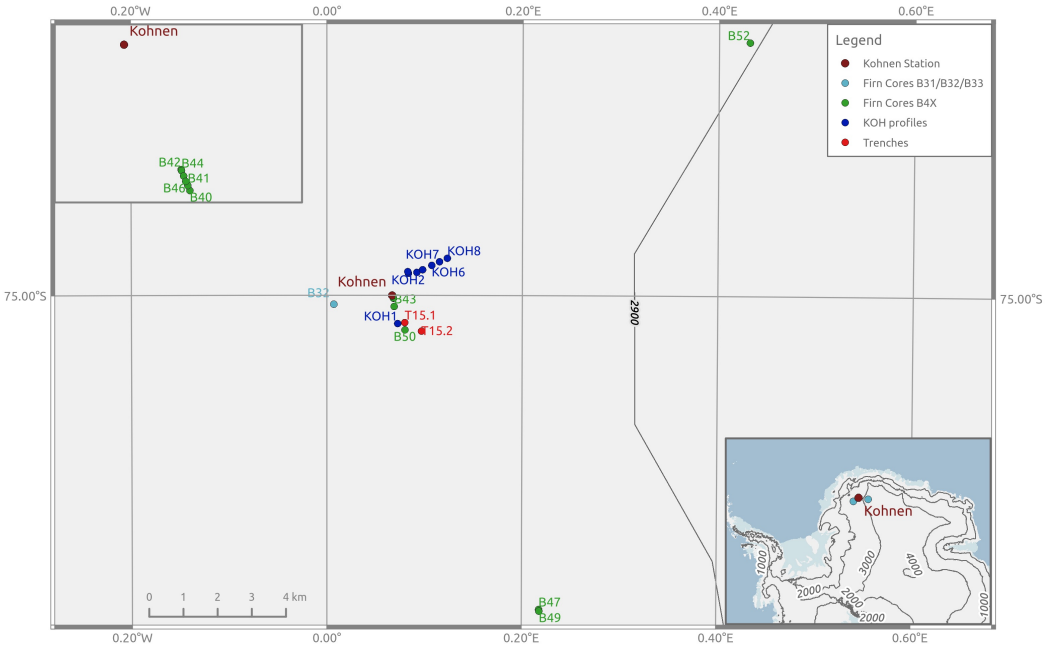

Figure 3.9.: Detailed map of all locations of analysed firn cores, snow pits and snow trenches listed in Table 3.2 and Table 3.3. An overview of the position on the Antarctic continent is given in the small panel on the right-hand side. In the upper left corner a detailed zoom on locations around Kohnen is shown.

Table 3.2.: Summary table about different surface snow samples and firn cores taken in DML. Elevations for B31, B32 and B33 are taken from Sommer et al. (2000), remaining elevation data are estimated from a digital elevation model (Bamber et al., 2009). Depth is divided into drilling depth and sampling depth in brackets, if the core is not entirely analysed. Further information on measuring, post-run correction and dating methods are given in the text.

Label	Date	Latitude °N	Longitude °E	Elevation (m a.s.l.)	Type	Depth (m)	Measuring Method	Post-Run Correction	Resolution (cm)	Dating	Reference
B31	1997-12-19	-75.5817	-3.4303	2669	firn core	115	IRMS	-	~10	lay. count.	[1, 2]
B32	1997-12-15	-75.00233	0.0070	2882	firn core	150	IRMS	-	~10	lay. count.	[1, 2]
B33	1998-01-07	-75.16700	6.4895	3160	firn core	130	IRMS	-	~10	lay. count.	[1, 2]
B40	S* 2012/13	-75.00073	0.0679	2891.7	firn core	200	CFA	-	1	lay. count.	[3]
B41	S 2012/13	-75.00071	0.0679	2891.7	firn core	110 (30)	CRDS	EvG	2	-	-
B42	S 2012/13	-75.00063	0.0678	2891.7	firn core	112 (30)	CRDS	EvG	2	-	-
B49	S 2012/13	-75.08357	0.2179	2893.5	firn core	114 (30)	CRDS	EvG	2	-	-
B50	S 2012/13	-75.00911	0.0798	2891.6	firn core	136 (30)	CRDS	EvG	2	-	-
KOH1	2012-12-03	-75.00744	0.0724	2891.6	snow pit	0.25	CRDS	EvG	0.5-1	-	-
KOH2	2012-12-09	-74.99411	0.0833	2891.7	snow pit	0.25	CRDS	EvG	0.5-1	-	-
KOH3	2012-12-17	-74.99368	0.0826	2891.7	snow pit	0.25	CRDS	EvG	0.5-1	-	-
KOH4	2012-12-24	-74.99387	0.0919	2892.2	snow pit	0.25	CRDS	EvG	0.5-1	-	-
KOH5	2012-12-31	-74.99317	0.0978	2892.5	snow pit	0.25	CRDS	EvG	0.5-1	-	-
KOH6	2013-01-06	-74.99201	0.1071	2892.5	snow pit	0.25	CRDS	EvG	0.5-1	-	-
KOH7	2013-01-11	-74.99105	0.1151	2892.5	snow pit	0.25	CRDS	EvG	0.5-1	-	-
KOH8	2013-01-18	-74.99013	0.1231	2892.9	snow pit	0.25	CRDS	EvG	0.5-1	-	-
T15-1	S 2014/15	-75.00719	0.0796	2891.6	trench	3.4	CRDS	piccr	2.2-3	-	[4]
T15-2	S 2014/15	-75.00944	0.0967	2892.0	trench	3.4	CRDS	piccr	2.2-3	-	[4]

[1] Oerter et al. (1999), [2](Graf et al., 2002), [3] Sigl et al. (2014), [4] Münch et al. (2017)
* S = season

New data

In addition to the above mentioned previously gained isotopic data, ten firn cores drilled in the austral summer season 2012/13 have been newly measured and analysed for this thesis. Information on the cores are given in Table 3.3, horizontal distance between the locations is given in Table 3.4. The total drilling depth of all firn cores varies. However, for this thesis the cores have been only measured and analysed at a resolution of 50 cm to a depth of 30 m. Hence, a sample at the top of a core represents about 2.5 years while a sample from the bottom contains snow of about 4 years. The depth-age-conversion is based on volcanic layers. It should be noted here that for the firn cores B41, B42 and B50 therefore two complementary data sets exist with different depth resolutions.

The preparation of the firn cores, i. e. cutting small pieces of 50 cm length from the 1-meter segments, was conducted in the ice laboratory at the AWI Bremerhaven. Prior to the measurement, the samples were kept in frozen state and subsequently thawed in a fridge at 4 - 7 °C. Afterwards, 1.6 ml of each sample was filled in a glas vial. Isotope ratios were measured using the CRDS method and a Picarro device in the isotope laboratory at the AWI Potsdam (Figure 3.6), operated with a 10 µl syringe injecting 2.1 µl per measurement. Each measurement sequence consisted of 47 to 52 vials in a rack of which the first eight vials as well as three vials inbetween and the last three vials were filled with standard waters. After the last injection the syringe was flushed with MilliQ water and 1-Methyl-2-pyrrolidon in order to clean the syringe and to extend the lifetime (Mikaela Weiner, personal communication). Raw data were calibrated following the piccr procedure. This post-run correction scheme was chosen in order to reduce the measuring time while keeping the same precision.

Elevation data for all locations are estimated using a digital elevation model for the AP (Bamber et al., 2009). Elevation data for B31, B32 and B33 differ between the absolute and the estimated values from the DEM. The calculated uncertainty of the DEM-derived data based on these three reference points is 11 m (RMSD). Consequently, elevation data are only presented to highlight relative elevation differences.

Table 3.3.: Summary of information on newly analysed firn cores. Elevation data are estimated from a digital elevation model (Bamber et al., 2009). Depth is divided into drilling depth and sampling depth in brackets. Further information on measuring, post-run correction and dating methods are given in the text.

Label	Date	Latitude °N	Longitude °E	Elevation (m a.s.l.)	Type	Depth (m)	Measuring Method	Post-run Correction	Resolution (cm)	Dating
B41	S* 2012/13	-75.00071	0.0679	2891.7	firn core	110 (30)	CRDS	piccr	50	volc. lay.
B42	S 2012/13	-75.00063	0.0678	2891.7	firn core	112 (30)	CRDS	piccr	50	volc. lay.
B43	S 2012/13	-75.00291	0.0687	2891.6	firn core	106 (30)	CRDS	piccr	50	volc. lay.
B44	S 2012/13	-75.00063	0.0678	2891.7	firn core	60 (30)	CRDS	piccr	50	volc. lay.
B45	S 2012/13	-75.00066	0.0678	2891.7	firn core	60 (30)	CRDS	piccr	50	volc. lay.
B46	S 2012/13	-75.00069	0.0679	2891.7	firn core	61 (30)	CRDS	piccr	50	volc. lay.
B47	S 2012/13	-75.08315	0.2177	2893.4	firn core	65 (30)	CRDS	piccr	50	volc. lay.
B48	S 2012/13	-75.00291	0.0687	2891.6	firn core	106 (30)	CRDS	piccr	50	volc. lay.
B50	S 2012/13	-75.00911	0.0798	2891.6	firn core	136 (30)	CRDS	piccr	50	volc. lay.
B52	S 2012/13	-74.93273	0.4313	2899.3	firn core	143 (30)	CRDS	piccr	50	volc. lay.

* S = season

Table 3.4.: Horizontal distances in km between drilling locations for the firn cores B40 to B52. Location for B43 lies close to the one of B48 and drilling site of B47 and B49 are also close together. Drilling location for B52 lies almost 13 km apart from all remaining sites.

	B52	B50	B49	B48	B47	B46	B45	B44	B43	B42	B41
B40	12.975	0.996	10.207	0.244	10.161	0.006	0.009	0.012	0.244	0.013	0.003
B41	12.975	0.999	10.21	0.247	10.165	0.003	0.006	0.009	0.247	0.01	
B42	12.973	1.009	10.22	0.257	10.174	0.007	0.004	0.001	0.256		
B43	13.1	0.762	9.977	0	9.932	0.25	0.253	0.256			
B44	12.973	1.008	10.219	0.256	10.174	0.006	0.003				
B45	12.973	1.005	10.216	0.253	10.17	0.003					
B46	12.974	1.002	10.213	0.25	10.167						
B47	17.888	9.17	0.047	9.932							
B48	13.1	0.762	9.977								
B49	17.929	9.215									
B50	13.277										

3.5. Stacking

Next to the comparison of different data sets, the overall aim of this thesis is to derive a reliable data set by improving the signal-to-noise ratio in the isotopic profiles. A method to reduce the non-climatic noise is to average several individual time series (e. g. several δ^{18}O profiles) to one timeseries (Fisher et al., 1985; Masson-Delmotte et al., 2015). Therefore all measured firn cores in this thesis are averaged to one stack. Figure 3.10 gives a schematic overview of all necessary working steps from a firn or ice sample itself to the final stack.

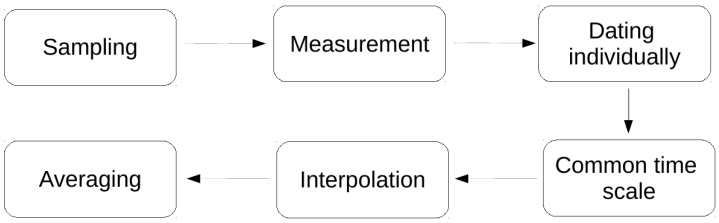

Figure 3.10.: Schematic overview of the steps done to build a stack from several firn cores.

After drilling, sampling and measuring e. g. firn cores (see Section 3.2), each core has to be dated individually (see Section 3.3). In order to treat every firn core in the same way in the final stack, an independent time scale must be selected. Each individual profile is interpolated to the chosen time scale. Finally, all data points for one point in time are averaged. Furthermore, it is necessary to interpolate and average the data set to obtain an equidistant temporal resolution because the initial temporal resolution varies with depth. Thus, a loss in variance in the high frequency range is inevitable.

In order to analyse this loss associated with each of the steps described above, numerical simulations are performed with surrogate data (white noise, 1,000 iterations). Results are presented in Section 4.3 according to the following scenarios:

- Case 0: A firn core with a length of 30 m and a sampling resolution of 1 cm is assumed. The time period is based on the upper 30 m of B40 and thus spans the interval from 1788 to 2010. Constant accumulation is assumed throughout the entire time span resulting in a yearly snow layer thickness of 13.5 cm, neglecting densification. One centimeter of snow then corresponds to 0.074 years throughout the entire core.

- Case 1: Initial conditions are the same as for case 0. The depth scale is converted to meter water equivalent (w. eq.) using the HL model (see Section 2.2 and 3.3) with an approximated surface density of 350 kg m^{-3}, an annual mean temperatures of -44.5 °C and a mean annual accumulation rate of 70 mm w. eq. yr^{-1}. The initial surrogate data set interpolated onto to the real depth-age scale.

- Case 2: Initial conditions are the same as for case 0. The data set is averaged to a sampling resolution of 50 cm (block average). The real depth is converted

to meter w. eq. using the HL model and assuming a constant accumulation rate of 70 mm w. eq. yr^{-1}. The time series is dated based on this accumulation rate and interpolated to an annual temporal resolution.

- Case 3: Initial conditions are the same as for case 0. The data set is averaged to a sampling resolution of 50 cm (block average). The real depth is converted to meter w. eq.. A real chronology taken from firn core B45 is assigned to the surrogate data, indicating a real temporal resolution with varying accumulation rates over time. From this varying temporal resolution a yearly data set is interpolated, hence, varying accumulation rates are considered.

- Case 4: Eleven white noise data sets as in case 0 are created. Varying accumulation rates are assumed. Each 'core' (time series out of surrogate date) is averaged (block averaged) to a resolution of 50 cm and dated according to temporal variations from firn cores B41, B42, B43, B44, B45, B46, B47, B48, B49, B50 and B52. All cores are interpolated to the independent time scale of B40 resulting in non-equidistant temporal intervals. Data are interpolated to an annual resolution.

4. Results and discussion

4.1. Differences in sampling and analysis methods

Here, it is analysed to which extent the isotopic values from the different data sets are affected by the different sampling, measuring and post-run correction techniques.

Analysis methods

A validation of the comparability between the post-run correction schemes EvG, E6inj and piccr is conducted to determine the discrepancy between them. None of the samples which are analysed in this thesis has been measured in both laboratories. However, reference waters are regularly exchanged. Both laboratories gauged these standards and obtained results within acceptable deviations. Thus, a comparison is conducted between the correction schemes E6Inj and piccr with a measurement from a CRDS device (Picarro L2130-i) in the isotope laboratory in Potsdam. For easier handling only waters with known isotopic ratios are measured.

The equipping of the measurement rack is carried out following the E6Inj method (Section 3.2). The detailed measurement sequence is shown in Figure A.1 in the Appendix. The rack contains 54 vials of which 32 are regarded as samples (tagged with 'S'), and 22 as reference waters which are separated into three blocks and used for the post-run correction.

Table 4.1 lists the oxygen and hydrogen isotopic ratios for all used reference waters. In order to quantify the drift manually, the injections four to six from each vial regarded as standards are averaged and the linear slope is calculated over the entire measurement time (Figure 4.1). The last measurement of reference water DML was rejected due to a measuring error (indicated in red). During the calibration, the data set is shifted and scaled to real isotopic values. Hence, raw data in Figure 4.1 differ from the desired values in Table 4.1. A small drift of on average 0.11 ‰ per measurement (~48 hours and 54 vials) is apparent with CoFi1 showing the greatest individual drift (0.28 ‰ per 54 vials). CoFi1 is also the lightest standard which has the greatest urge to fractionate into the headspace in the vial. Thus, the overall drift is strongly influenced by CoFi1.

For calibrated data, a deviation up to 0.1 ‰ for δ^{18}O and 0.8 ‰ for δD measurements is in the range of the expected measurement uncertainty (Hanno Meyer, personal communication) and therefore acceptable. The δ^{18}O value for TD2 shows a deviation to the predefined value of -0.08 ‰ for E6Inj and -0.06 ‰ for piccr. Both results are thus within the measurement uncertainty. By subtracting the measured values from the desired values, resulting deviations reveal a slope of 0.02 ‰ per 54

Table 4.1.: Raw data for oxygen and hydrogen isotopic ratios used for the comparison between Excel-based and R-based post-run correction. TD2 is only used for quality control and not for calibration purposes.

Label	δ^{18}O [‰]	δD [‰]
TD1	-33.92	-267.7
DML	-45.50	-341.0
TD2	-45.12	-362.2
DOME-C1	-46.52	-372.8
CoFi1	-52.94	-412.4

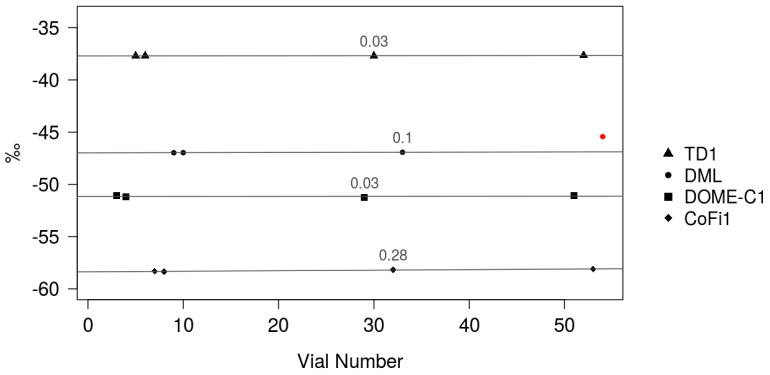

Figure 4.1.: Raw data of reference waters from the Picarro measurement used for memory- and drift-correction and final calibration. The x-axis shows the respective vial number. Each point represents an average over the last three injections per vial. Horizontal lines and numbers indicate the trend over the entire measurement (~48 hours) for the respective standards TD1, DML, DOME-C1 and CoFi1.

vials for E6Inj and -0.12 ‰ per 54 vials for piccr.

The root mean square deviation (RMSD) is calculated to measure the differences between two data sets with the equation

$$RMSD = \sqrt{\frac{\sum_{i=1}^{n}(x_i - y_i)^2}{n}} \tag{4.1}$$

with n being the length of the respective data sets x and y and $i = 0, 1, ..., n$. The RMSD between the measured and the reference values is 0.11 ‰ for E6Inj and 0.12 ‰ for piccr. Between both calibrated data sets the RMSD amounts to 0.08 ‰. The overall deviation between measured and true values is thus slightly above the expected measurement uncertainty. However, both schemes deliver comparable results for the same data set allowing a direct comparison of differently calibrated firn core data sets.

High vs. low resolution data

Since the slight differences between the presented correction techniques are around the measurement uncertainty, it is possible to compare high resolution measurements (2 cm) calibrated with EvG to low resolution measurements (50 cm) calibrated with piccr. For the firn cores B41, B42, and B50, data sets exist at both resolutions

(Tables 3.2 and 3.3). The following analysis presents only firn core B42 because missing data complicate the comparison. Nevertheless, the result is representative for all three cores; detailed plots for B41 and B50 are shown in the Appendix (Figures A.2, A.3 and A.4).

The 2 cm data set is averaged to 50 cm sequences and compared to the low resolution measurement. This comparison is illustrated for firn core B42 in Figure 4.2. The high resolution data (orange) reveal short-scale variability which is no longer evident in the low resolution timeseries. In the depth from 3 to 5 m, the averaged data (red) show a remarkable deviation from the low resolution measurement (blue). Missing data points in the high resolution record cause a biased average, resulting in a larger deviation and lower correlation (0.94, pairwise Pearson correlation coefficient) between both timeseries. However, Figure 4.3 indicates that the deviation is not a systematic offset between both laboratories. By neglecting these data points, the agreement with correlations above 0.99 for δ^{18}O and δD support the conclusion that the low resolution data represent very well the overall behaviour of the high resolution timeseries for the case study of firn core B42.

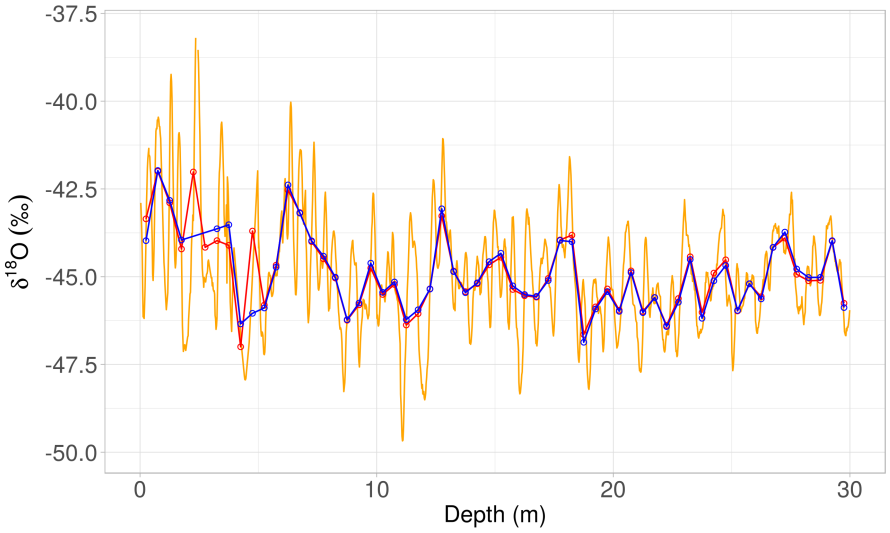

Figure 4.2.: Comparison of the 2 cm resolution data set (orange), hereof a 50 cm average (red) and the 50 cm resolution measurement (blue) for B42. Differences in the depth interval from 3 to 5 m are caused by missing data points in the high resolution timeseries. In general, low resolution measurements agree well with averaged data.

Reference water TD2, which is used in the new measurements for quality control, shows a RMSD between the reference and the measured values of 0.06 ‰. The RMSD for oxygen isotopes between the averaged data and the 50 cm measurements for B42 is 0.13 ‰ (neglecting data between 3-5 m depth). Table A.1 gives detailed information on correlation coefficients and RMSDs for B41, B42 and B50. Furthermore, a t-test based analysis between averaged and low resolution timeseries reveals no significant difference for all three firn cores.

Summarising the presented comparisons (Figures 4.2 and 4.3 as well as Figures and Table in the Appendix) allow us to conclude that there is no systematic difference between measurements from different isotope laboratories applying different

measuring and post-run correction schemes. Due to time constraints, B49 was not cut to a 50 cm resolution and here an averaged data set of the 2 cm resolution data is used. B50 has missing data in the low resolution timeseries which are filled with averaged data from the high resolution measurement.

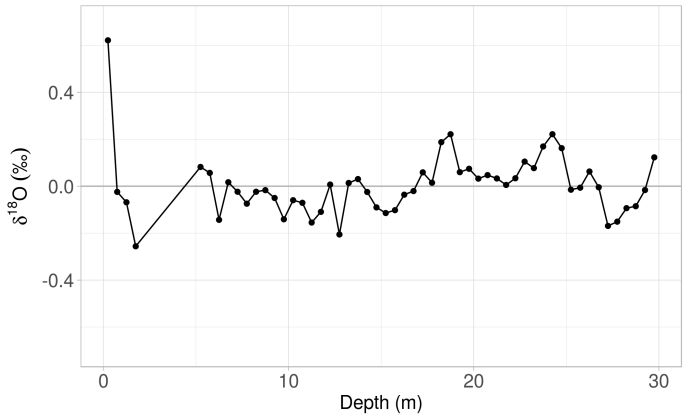

Figure 4.3.: Deviations between averaged high resolution (2 cm) and low resolution (50 cm) measurements for B42. No systematic difference between both data sets is evident. Note that the data between 3 and 5 m depth have been removed here due to missing data points in the high resolution timeseries.

Sampling and measuring methods

In the following, differences between discrete (CRDS, Picarro device) and continuous measurements (CFA system) are addressed comparing the power spectral density (PSD) of B40 to the average of the individual spectra of B41, B42, B49 and B50. Furthermore, we compare the spectrum of the average trench profiles from T15-1 and T15-2 to the average firn core spectrum in order to investigate possible effects of sample collection and storage. Due to the limited depth of the trenches, only the upper three meter of each data set are analysed which cover approximately the last 20 years. Information on the measured resolutions and used post-run correction schemes are presented in Table 3.3.

A spectrum is chosen because it provides information on the distribution of power in frequency components. The multitaper method after Percival and Walden (1993) is used for the spectra shown in Figure 4.4. Horizontal distances between all sampling positions are less than 10 km (Figure 3.9, Table 3.4). Deviations in the frequency domain due to temporal or spatial changes in climatic conditions are therefore not expected.

The here analysed data sets were measured in different resolutions. This fact is responsible for the varying drops of the spectra around 0.15 cm^{-1}, 0.25 cm^{-1} and 0.5 cm^{-1} for the trenches, the discretly measured firn cores and the continuously measured core B40, respectively. Furthermore, the spectrum for B40 (Figure 4.4, black) shows a deviation from the average spectrum for firn cores B41, B42, B49 and B50 (turquoise) in the frequency range from 0.05 cm^{-1} to 0.2 cm^{-1}. The decrease between 0.04 cm^{-1} and 0.07 cm^{-1} is relatively similar in both spectra. Besides that, discrete firn core measurements show a lower PSD in the lower frequency range

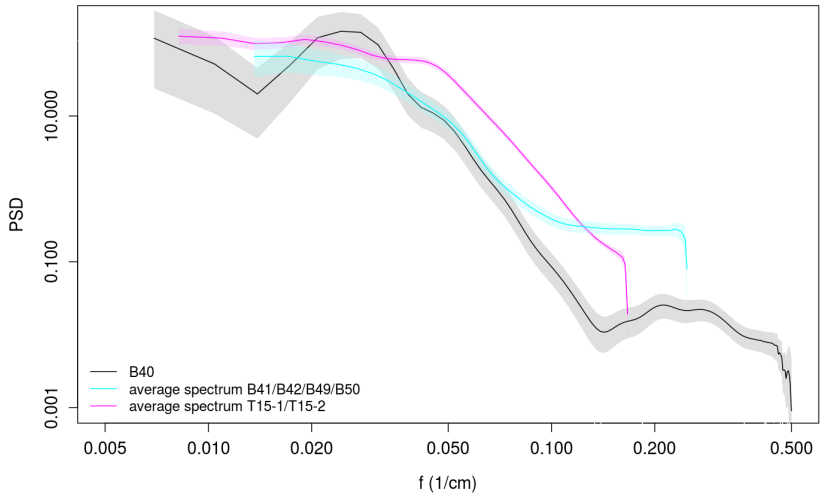

Figure 4.4.: Power spectral densities (PSD) for B40 (continuously measured, CFA, black) as well as for all trench trench profiles from T15-1 and T15-2 (discrete measurements, CRDS, pink) and firn cores B41, B42, B49 and B50 (discrete measurements, CRDS, turquoise) are shown based on the multitaper method (Percival and Walden, 1993). All spectra are smoothed and confidence intervals are shown. All 22 single trench-profile spectra as well as the spectra from the discretely measured firn cores are averaged, respectively. Only the upper 3 m of the profiles are analysed.

($< 0.15\,\mathrm{cm}^{-1}$) than the average spectrum from the T15-1 and T15-2 (Figure 4.4, pink). Around $0.15\,\mathrm{cm}^{-1}$ the latter spectrum shows a fast decrease while the average spectrum from the firn cores remains at the same PSD.

The blurring effect due to melting in a CFA system leads to indistinct peaks and reduced amplitudes (Kirstin Hoffmann, personal communication) which might explain the apparent lower spectral density in the spectrum of B40 on the high-frequency side ($> 0.07\,\mathrm{cm}^{-1}$). Snow trench samples are packed individually whereas firn core segments are stored unsealed in polystyrene boxes. Subsequent diffusion or other processes happening after the sampling and during the storage might be a possible reason for the above mentioned differences in spectral densities.

4.2. Spatial variability on local to regional scales

Eight 25 cm deep profiles (KOH1 to KOH8) are analysed in order to learn about spatial variations in the surface snow. Due to the distances of about 1 km between each sampling site (see Figure 3.9), it is assumed that the stratigraphic noise is not correlated whereas the climate signal is considered to be the same (Münch et al., 2016). All eight profiles were sampled within six weeks (see Table 3.2). Meteorological conditions measured at the nearby AWS 9 during this period reveal no substantial weather changes (e. g. strong wind events, warm periods, precipitation or snow fall events) which could strongly alter the isotopic composition of the upper 25 cm of the snow cover (see Figure B.1 in the Appendix). Elevations for the sampling positions are estimated (Table 3.2) from a digital elevation model (Bamber et al., 2009) and indicate a flat area.

Mean and standard error for each isotopic profile are compared (Figure 4.5 a)) assuming an effective number of samples of three due to autocorrelation of the data. Mean values range from -48.84 ‰ (KOH1) to -44.39 ‰ (KOH8). The latter profile shows the largest standard error (3.51 ‰). Furthermore, the study from Münch et al. (2017) analysed the snow trenches T15-1 and T15-2 and highlighted the contribution of stratigraphic noise leading to varying horizontal layers and patchy features at the snow surface. Assuming therefore that the uncertainty of the mean is caused by e. g. stratigraphic noise, the doubled standard deviation of the means of all trench profiles across the uppermost 25 cm (Figure 4.5 b)) yields that all KOH profiles are not significantly different. Hence, the slight differences in the mean might be due to local topography, e. g. small dunes.

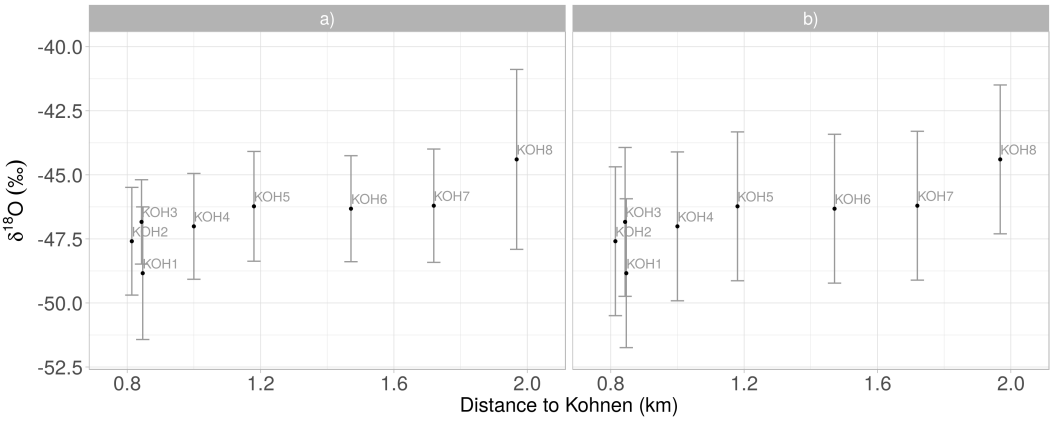

Figure 4.5.: Mean values for the snow pits KOH1 to KOH8 against the distance to the Kohnen research station. Errobars indicate a) the respective standard error assuming an effective number of samples of three, and b) the doubled standard deviation of the overall mean from T15-1 and T15-2 (see text). No systematic difference in δ^{18}O values is evident.

Following this short-scale analysis, spatial variability across different depth intervals in the firn cores B40 to B52 are studied. For this, mean values and the respective standard error are calculated for the depth intervals 0 - 4 m, 4 - 10 m, 10 - 20 m, 20 - 30 m (Figure 4.6). The maximum distance between sampling sites is ~15 km (see Figure 3.9). The uppermost depth interval from firn core B40 agrees to neighboring profiles; however, δ^{18}O values from 4 to 30 m depth show large deviations from the general isotopic compositions. As a result of this, the timeseries of B40 is not used for further analysis. Furthermore, relatively high δ^{18}O values are evident as a general pattern in the depth interval from 0 to 4 m. B41, B42, B44, B45 and B46 show the highest mean values up to -43.3 ‰, whereas B47 and B49 remain at the same level. Additionally, firn cores B43 and B48 indicate in each depth interval a very similar behaviour. Both cores are drilled very close to each other as shown in Table 3.4. Similar pattern are evident for firn cores B47 and B49, which are also close to each other, as well as for the above mentioned group from B41 to B46. The drilling site B52 lies more than 12 km away from all remaining sites and, however, shows slightly higher values for each depth interval.

Consequently, profiles from neighboring cores are more similar to each other than

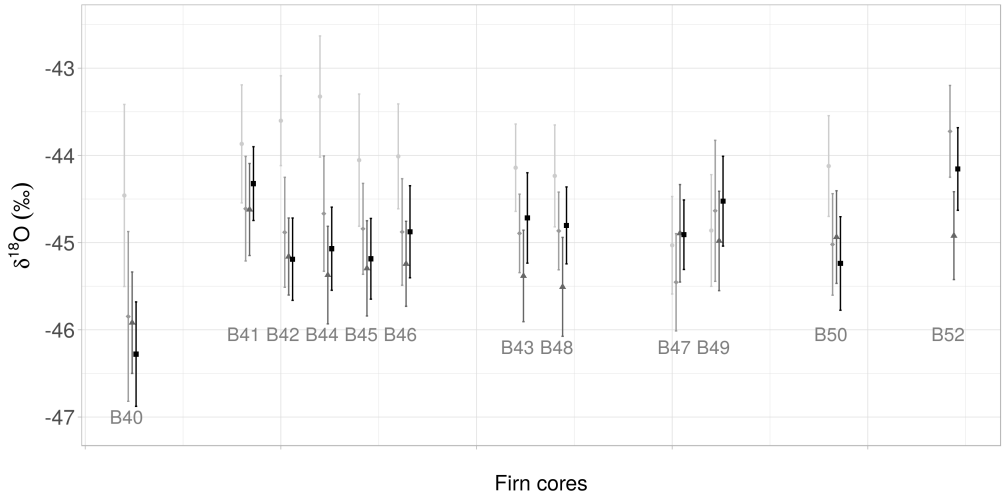

Figure 4.6.: Horizontal variability of mean values for different depth intervals from all firn cores around Kohnen. Dots show the mean value and bars the standard error for the depth intervals: 0 - 4 m, 4 - 10 m, 10 - 20 m, 20 - 30 m (from left (light grey) to right (black)). Grouping indicates cores which are close to each other. Side by side located cores show similar patterns while B40 deviates from the general behaviour, especially in the deeper intervals. Note that for B52 data are missing for the upper 3 m.

to profiles far away. Changing values with depth can be an indication for changing climatic conditions or alternating wind- or precipitation-pattern. It can further be assumed that B52 experiences slightly different accumulation conditions through the spatial distance to the remaining firn cores. Differences due to the measuring methods can be excluded because all samples (expect for B40) are measured in the same way. However, the preparation in the ice laboratory was done at different dates. An effect of sample storage is yet not mentioned in the literature.

4.3. Temporal variability of stable water isotopes

A reliable chronology is essential for each firn or ice core. The dating procedure based on volcanic layers (Section 3.3), is applied in the following. Afterwards, the temporal behaviour of all analysed firn profiles is presented before the formation of the final stack is illustrated. Mean annual accumulation rates are derived and variations are compared to the variability of δ^{18}O values. Moreover, a comparison to previously analysed cores is conducted and theoretical considerations on the amount of remaining frequency after stacking are explained. In the end, the conversion from δ^{18}O to temperature is conducted and decadal trends are derived and discussed.

Dating

The volcanic layer dating scheme is applied because no impurity measurements are available. The electrical conductivity was measured at the AWI Bremerhaven. Distinct peaks in these data were ascribed to four prominent volcanic events (Delmas

et al., 1992) during the last 200 years taking into account a shift in time due to the temporal difference between eruption and deposition. These eruptions are volcano Agung in 1963, volcano Krakatoa in 1883, volcano Tambora in 1815 and an unknown volcanic eruption in 1809 (Karlöf et al., 2000; Oerter et al., 2000). The respective depths of the ash layers in meter w. eq. for each firn core are listed in Table 4.2.

Figure 4.7 shows examplarily the conductivity profiles of B40, B47 and B50. The two prominent peaks between 10 and 15 m w. eq. indicate the volcanic events Tambora in 1815 and the unknown volcano in 1809. Agung (1964) and Krakatoa (1884) caused weaker but still visible peaks in the conductivity profiles. Individual depth-age conversions for each core are important due to differing depths of volcanic horizons, as it is evident in Figure 4.7 and are the result of different accumulation rates in DML.

Table 4.2.: Depths of peaks (m w. eq.) in conductivity profiles indicating volcanic horizons which are used as time markers. For B43 the eruption of Krakatoa was not clearly identifiable.

Name	Date	B40	B41	B42	B43	B44	B45
Agung	1964	3.617	3.690	3.565	3.606	3.566	3.584
Krakatoa	1884	8.866	8.791	8.746	-	8.755	8.786
Tambora	1815	13.302	13.206	13.212	12.215	13.206	13.218
Unknown	1809	13.709	13.593	13.599	12.599	13.606	13.625

Name	Date	B46	B47	B48	B49	B50	B52
Agung	1964	3.379	2.982	3.919	3.416	3.531	3.375
Krakatoa	1884	8.553	7.419	8.984	7.847	8.845	8.584
Tambora	1815	12.986	11.227	13.201	11.692	13.345	12.852
Unknown	1809	13.383	11.567	13.651	12.052	13.725	13.253

The presented volcanic eruptions mark tie points in time; within these dates the temporal scale is linearly interpolated. No extrapolation before the first tie point (1809) is conducted and the depth-age scale therefore ranges from 1809 to 2012, the drilling date. However, the layer of the eruption from Krakatoa in 1884 is not visible at all in the conductivity profile of B43. Thus, the largest interpolated period is about 80 years in general and 149 years for B43.

The dating uncertainty of these interpolated timescales is estimated by comparing the interpolated timescale of B40 to the published B40 timescale based on annual layer counting of impurity data (Sigl et al., 2014). This yields a maximum deviation of 3.2 years and an average dating uncertainty of 1.9 years (RMSD).

Next to the spatial variations, also temporal variations can be addressed based on the depth-age conversion. Figure 4.8 shows isotope profiles over time for all eleven firn cores B41 to B52. Peaks are not completely simultaneous due to the varying temporal resolution caused by the fact that the fixed sampling resolution of 50 cm corresponds to slightly different temporal intervals due to the varying depth-age scales of the cores. Furthermore, the dating uncertainty can cause discrepancies as

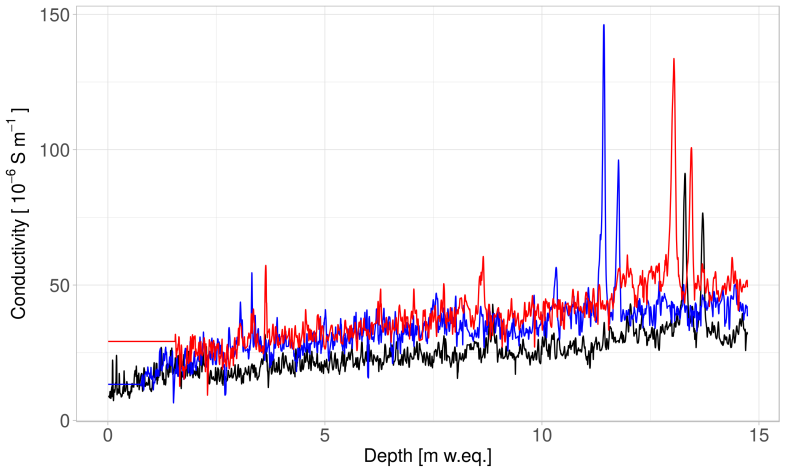

Figure 4.7.: Electrical conductivity data for the upper 30 m from firn cores B40 (black), B47 (blue) and B50 (red). The two prominent peaks between 10 and 15 m w.eq. indicate the eruptions of Tambora 1815 and the unknown volcanic event in 1809.

well. However, the overall temporal behaviour is relatively similar (Figure 4.8).

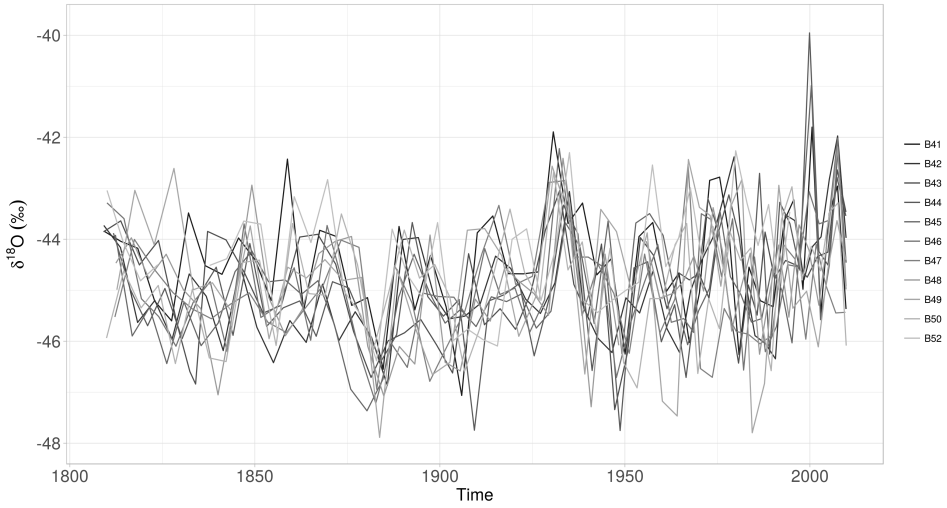

Figure 4.8.: Stable oxygen isotopes over time for the period of investigation from 1809 to 2012 for firn cores B41 to B52. Peaks are not completely simultaneous (see text); however, the overall behaviour of the isotopic composition of all firn cores is similar.

Derived mean annual accumulation rates and connection to oxygen isotopes

Dividing a depth interval (m w. eq.) by the respective time difference (years) yields the mean annual accumulation rate for the specific time period and the respective site. In this thesis, mean annual accumulation rates are derived for the periods between volcanic eruptions. Accumulation rate with a higher temporal resolution require annual layer counted chronologies.

Mean annual accumulation rates for the entire period of investigation are ~66 mm w. eq. yr^{-1} which agree well with previously published values from DML (e. g. Oerter et al., 2000; Sommer et al., 2000). However, lower accumulation rates are found for

the period before 1964 (~62 mm w. eq. yr^{-1}) and higher values afterwards (~78 mm w. eq. yr^{-1}, Table 4.3). Figure 4.9 shows individual mean annual accumulation rates for each firn core and each time interval between volcanic eruptions. Single profiles deviate from the general trend towards higher mean annual accumulation rates: B47 and B49 indicate lower rates throughout the last 200 years while B52 shows comparatively high values for this region. A dating error for the volcanic ash layer of Agung 1964 could not be responsible for this huge shift in mean annual accumulation rates due to the small dating uncertainty of about 3 years.

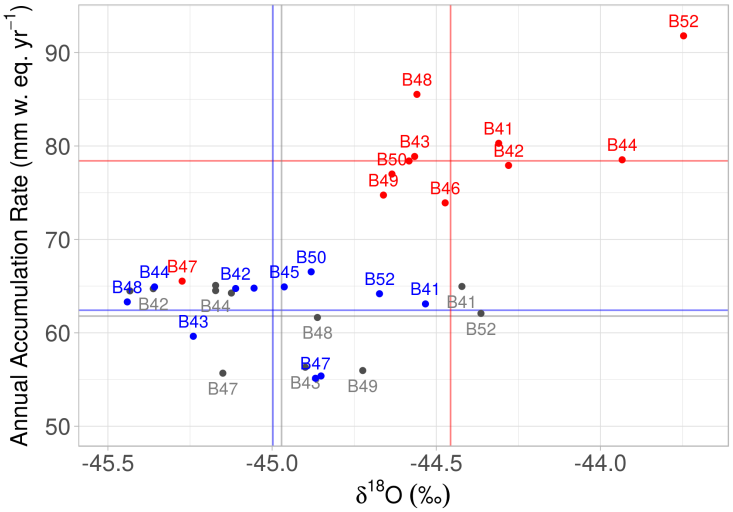

Figure 4.9.: Relation between $\delta^{18}O$ and mean annual accumulation rates for the periods before 1884 (grey), 1884 to 1964 (blue) and after 1964 (red). The vertical and horizontal lines indicate averages over all firn cores for the respective parameter and period of time. Note that for firn core B52 $\delta^{18}O$ values for the upper three meter (i. e. 1994 to 2012) are missing.

Based on these findings an increase in accumulation rate of about 25 % is evident. The pattern of decreased accumulation rates during the 19th and increased rates during the 20th century is already mentioned in several studies as e. g. in Oerter et al. (1999). Next to the temporal variability of mean annual accumulation rates, variations of oxygen isotopes are shown in Figure 4.9 and Table 4.3 as well and indicate mostly a similar behaviour as the accumulation rates. There might be a (linear) relation between mean annual accumulation and the isotopic composition. However, both parameters are influenced by other parameters, a reliable conclusion is therefore not possible. Furthermore, the presented differences between individual firn cores demonstrate once more that one single profile is not representative to derive general trends for a wider area.

Table 4.3.: Statistical summary of oxygen isotope data and derived mean annual accumulation rates for firn cores B41 to B52. Isotope data and accumulation rates are separated for the particular time periods before 1884, from 1884 to 1964 and after 1964. Dates rely on volcanic match points. SD = standard deviation; Var = variance.

Label	Mean (‰)	SD (‰)	Var ((‰)^2)	Mean (‰)			Mean Annual Accumulation Rate (mm w. eq. yr^{-1})			
				<1884	1884-1964	>1964	1809-2012	<1884	1884-1964	>1964
B41	-44.43	1.07	1.14	-44.42	-44.53	-44.31	67.71	64.93	63.10	80.29
B42	-44.92	1.05	1.10	-45.36	-45.11	-44.28	67.73	64.72	64.75	77.92
B43	-44.90	0.99	0.97	-44.90	-45.24	-44.57	62.77	56.32	59.63	78.88
B44	-44.84	1.28	1.63	-45.17	-45.36	-43.93	67.88	64.52	65.00	78.52
B45	-44.98	1.09	1.19	-45.43	-44.96	-44.58	67.85	64.49	65.00	78.40
B46	-44.87	1.07	1.15	-45.12	-45.06	-44.47	66.66	64.26	64.78	73.91
B47	-45.03	0.93	0.87	-45.15	-44.87	-45.27	57.70	55.68	55.14	65.53
B48	-44.99	1.13	1.28	-44.86	-45.44	-44.60	67.83	61.64	63.31	85.53
B49	-44.75	1.35	1.83	-44.72	-44.85	-44.66	60.08	55.96	55.38	74.74
B50	-44.95	1.05	1.09	-45.17	-44.88	-44.64	68.36	65.08	66.53	77.00
B52	-44.38	1.02	1.03	-44.36	-44.67	-43.74	66.81	62.08	64.18	91.79
$\sum$	-44.82	1.09	1.21	-44.97	-44.99	-44.46	65.58	61.80	62.42	78.41

Spatial correlation pattern

Münch et al. (2016) studied the spatial correlation structure on a scale from 1 m to 500 m by analysing two 1 m deep snow trenches. Further, they simulated the probability to detect a linear temperature trend in a single isotopic profile which lies between 10 and 25 %. Averaging across several cores reduces the amount of non-climatic effects in the data set of which stratigraphic noise is the major contribution to the horizontal isotopic variability. In this thesis, the presented study from Münch et al. (2016) is reproduced while extending the scale to 15 km by analysing the spatial correlation structures between the firn cores B41 to B52 based on isotopic profiles in absolute depth.

In particular, significant correlation coefficients between 0.4 and 0.69 are evident for horizontal spacings below 10 m (Figure 4.10). Correlations decrease at distances greater than 10 m, reaching constant values around 0.3 to 0.35 for pairs which lie 1 km away from each other. Isotopic profiles with spacings of about 10 km show only low correlations which are not significant.

The observed spatial correlation structure was to be expected with regard to the results in Münch et al. (2016). High correlations between neighboring profiles indicate that isotopic variations are dominated by common stratigraphic noise which decreases with increasing distances. It is therefore recommended to stack profiles from locations with a minimum spacing of 10 m to achieve the best possible data set.

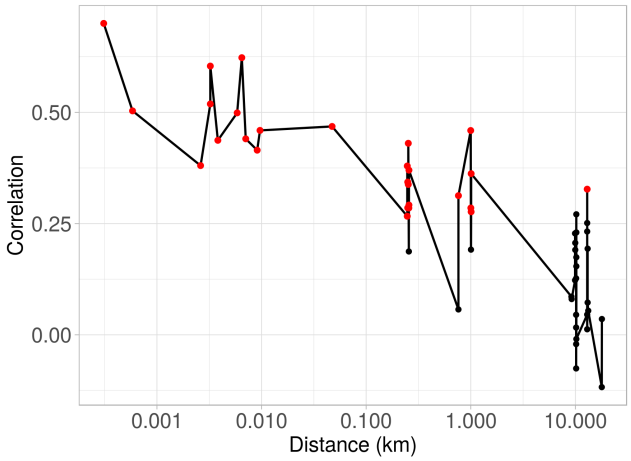

Figure 4.10.: Correlations as a function of distance (logarithmic scale) for all possible profile pairs from the eleven firn cores B41 to B52. Red dots indicate significant correlations on the 95 % level. Highest correlations up to 0.69 are found for pairs with horizontal distances of less than ten meter. Correlations decrease with increasing distance between profile pairs and are not significant at spacings of ~10 km.

Deriving a reliable data set – Stacking

Analyses from single firn or ice cores are neither sufficient to investigate recent temperature trends (Münch et al., 2016) nor are they representative for a wider area (Fisher et al., 1985; Karlöf et al., 2006; Richardson-Näslund, 2004). In order to

reliably deduce temperature variations during the last 200 years, all measured firn cores (B41 to B52) are therefore combined to one stack. The applied procedure is schematically illustrated in Figure 3.10 in Section 3.4.

Since the isotopic data from B40 are not used due to large deviations (Figure 4.6) to all remaining isotopic data, the timescale of B40 is used as the common independent timescale for the final stack. Thus, every firn core is treated in the same way with respect to interpolation and averaging. The question how the distribution of spectral power changes due to stacking is theoretically described in Section 3.5 and illustrated in Figure 4.11. Case 0 represents the pure raw data whereas in case 1 the logging depth is converted to w. eq. and the timeseries is interpolated to equidistant spacings. Hence, the spectral density decreases for very high frequencies. Case 2 considers a temporally constant sampling. The drop at 0.25 yr^{-1} is the results of the sampling resolution of 50 cm. A real dating according to firn core B45 is conducted in case 3, showing a slightly weaker drop at 0.25 yr^{-1} compared to case 2. Finally, case 4 represents the stack and shows further loss of spectral power.

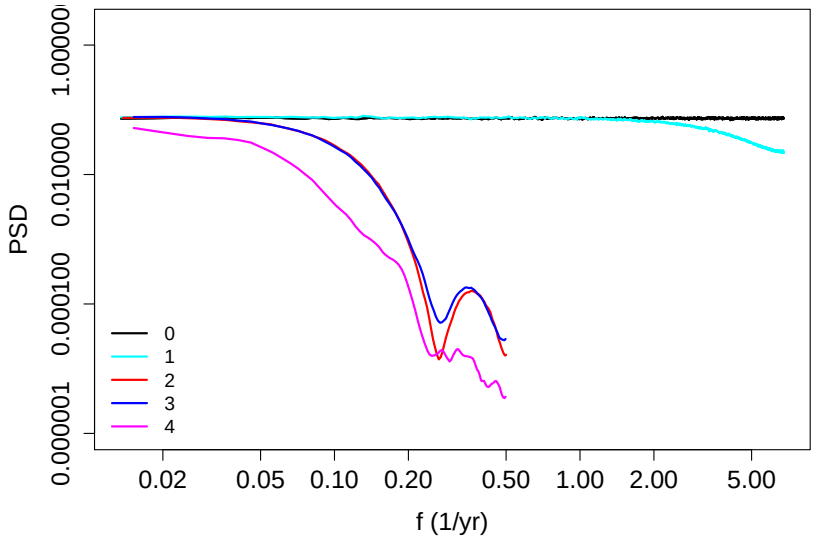

Figure 4.11.: Power spectrum for differently processed surrogate data analysing the effect of averaging and interpolation on a time series. Cases 0 to 4 are explained in Section 3.5. Note that both axes are logarithmic.

Table 4.4 shows variances associated to the above presented cases. As Figure 4.11 indicates, one third of the variance loss happens in the high frequency range between case 0 and case 1. In general, variances decrease more and more between the cases 2, 3 and 4 corresponding to an increasing loss of information in the respective data set, both is caused by averaging and interpolation. This is both evident for the total, but also for decadal and the multi-decadal (< 50 years) variances. Case 4 corresponds to the stack which is developed in this study. Therefore, about 30 % of the total decadal variance is preserved in the stack and even 48 % on a multi-decadal scale.

In conclusion, the initial sampling resolution together with processes as averaging and interpolation reduce the variance in a timeseries especially in the high frequency ranges. Nevertheless, it can be assumed that the here analysed stack still contains enough information to ensure reliable conclusions, especially because the main in-

Table 4.4.: Total, decadal and multi-decadal (50 years) variances ($(‰)^2$) for differently processed data. Cases 0 to 4 are explained in Section 3.5, the associated plot is shown in Figure 4.11. On a multi-decadal scale, an interpolated and averaged data stack still contains almost 50 % of the initial variance.

Case	Total	Decadal	Multi-decadal
0	1	1	1
1	0.666	1	1
2	0.012	0.74	0.93
3	0.012	0.73	0.92
4	0.004	0.30	0.48

terest lies in the overall trend during the last two centuries.

Temporal variability of the δ^{18}O stack

The analysis of the loss of spectral density in each step yields, nevertheless, that the stack from all eleven firn cores contains still enough variance to present a reliable timeseries of δ^{18}O variability during the last 200 years. It is now addressed whether a trend is evident and if so, whether this trend is of an anthropogenic origin or a continuation of a natural climate variation.

The resulting temporal timeseries is shown in Figure 4.12 with a mean value of -44.9 ‰ and a standard deviation of 0.624 ‰. A δ^{18}O minimum is apparent around 1880 with -46.5 ‰. The highest value is obtained around the year 2007 with -43.0 ‰, the second highest around 1935 with -43.7 ‰. Seasonal cycles are not preserved due to the sampling resolution of 50 cm.

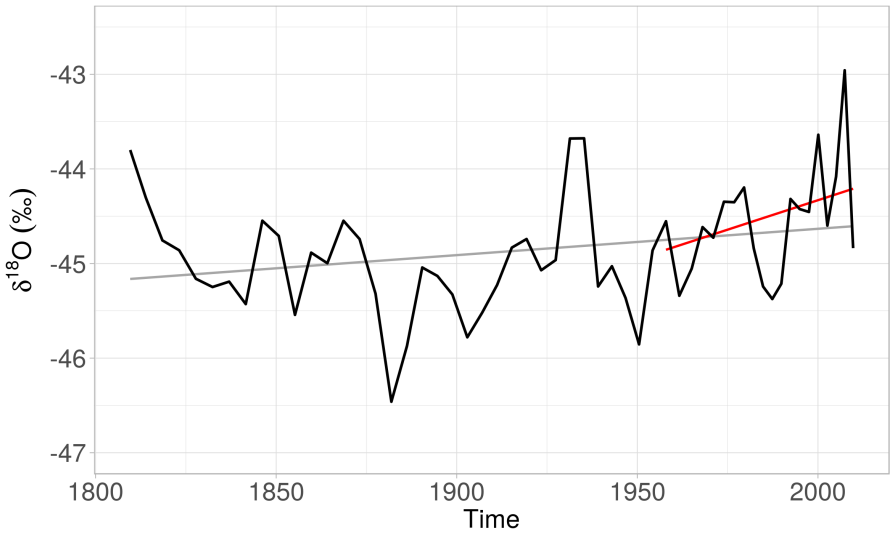

Figure 4.12.: Temporal variability of the stacked data set (firn cores B41 to B52) for the time period from 1809 to 2012 (black). A linear regression model reveals a significant positive slope of 0.56 ‰ over the entire period (grey) and a slope of 0.65 ‰ for the period between 1957 and 2012 (red).

Comparing the individual profiles (Figure 4.8) to the stack reveals that almost every profiles shows a minimum isotopic ratio around 1880 and a maximum around

1935. Hence, the stack is not biased by single strong influencing cores. A significant trend on the 99 % level of 0.56 ‰ δ^{18}O over the entire period of investigation (1809 to 2012) is found, equivalent to a trend of 0.03 ‰/10 years. Regarding the time after 1957, we find a trend of 0.65 ‰, equivalent to 0.13 ‰ per decade, but is however not significant. According to the published relationship between δ^{18}O and temperature for DML of 0.8 ‰/Kelvin (e. g. Oerter et al., 1999; Touzeau et al., 2016), the converted temperature trend considering the entire period of investigation is 0.70 °C/decade. For the period after 1957, the converted δ^{18}O increase indicates a trend of 0.16 °C/decade.

Steig et al. (2009) suggested a warming trend of 0.10 ± 0.07 °C per decade over East Antarctica for the period from 1957 to 2006 based on reconstructed temperature anomalies from satellite thermal infrared measurements validated with data from AWSs. Considering both results, the one from Steig et al. (2009) and the conclusions from this thesis, a positive temperature trend can be concluded at least for the last 50 years. However, in order to investigate the origin of the recent change – anthropogenic or natural – a comparison between the stack and data from the last 1000 years in conducted.

For this, B31 and B32 are averaged in the same way as it was done for the stack, B33 is not used as the timeseries shows too large deviations in the mean to B31 and B32 due to differences in the location (see Table C.1 in the Appendix). The initial timeseries are individually converted to depth intervals of 50 cm, interpolated to the timescale of B40 and averaged which is possible because B40 is dated until 500 BC (Sigl et al., 2014, supplementary material). Figure 4.13 illustrates both stacked data sets for the last 1,000 years. Oxygen isotopic ratios above -44 ‰ are rare whereas the new stack might indicate a slight trend towards higher isotopic values. The correlation for the overlapping period from 1810 to 1987 is 0.465.

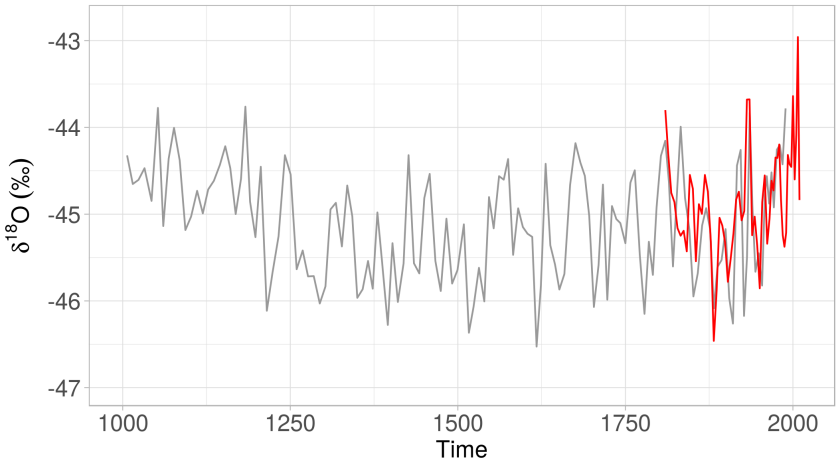

Figure 4.13.: Comparison of the temporal variability of δ^{18}O between data covering the period form 1000 to 1950 (B31 and B32, grey) and the new stack (1809 to 2012, red). Averages above -44 ‰ are rarely apparent during the last millennium, but more frequent in the 20th.

By comparing histograms of both stacks (Figure 4.14), the question whether the recent changes in isotopic values deviate from natural variability can be assessed.

The considered time interval for the B31-B32 stack ranges from 1000 to 1950 in order to highlight the period after 1950. The overall mean value for the B31-B32 average is -45.15 ‰, for the new stack -44.85 ‰, standard deviations are 0.63 ‰ and 0.62 ‰, respectively. A t-test reveals that both data sets have significantly different mean values ($p = 0.004$).

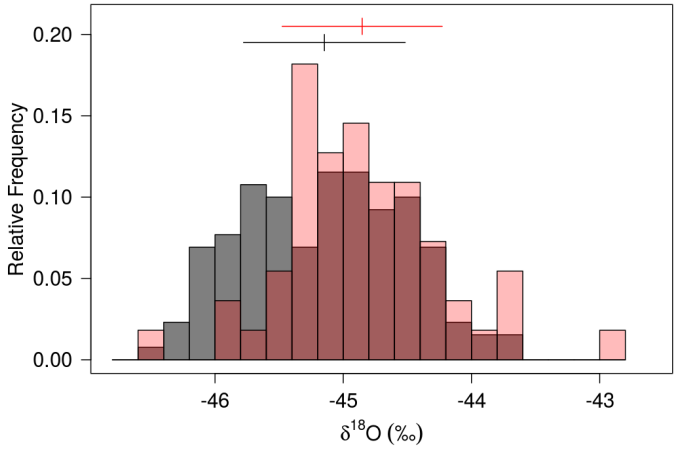

Figure 4.14.: Relative frequencies of $\delta^{18}O$ values for the averaged data set of B31 and B32 (grey) for the time period from 1000 to 1950 CE compared to the stacked data set covering the time from 1809 to 2012 (red). The vertical and horizontal bars on top indicate the mean and the respective standard deviation of each stack. The data indicate a slight shift towards higher isotopic ratios for the more recent data set.

Jouzel et al. (1997) pointed out, that recorded temperatures during precipitation events may not necessarily be representative for the annual mean temperature. Changes in the seasonality of snow fall, e. g. higher precipitation in summer than in winter, can result in misleading findings of increased temperatures. In summary, the results obtained in this thesis suggest a trend during the last 50 years in DML, however, we cannot say for sure whether this trend is a real rise in temperatures.

5. Conclusions and outlook

In this thesis, published and new water isotopologue data from snow pits, snow trenches and firn cores have been comprehensively analysed and compared. In the following, the main findings of this work are summarised and a final outlook is presented which highlights possibilities for future work.

Differences between sampling, measuring and post-run correction methods

Discrepancies between continuous and discrete measuring methods and between drilled and manually taken samples have been observed analysing the respective power spectral densities (Figure 4.4). It is not entirely clear whether the lower variance in the high frequency range of data measured continuously in a CFA system are due to a more pronounced smoothing during the measurement. Differences between discrete measured firn core samples and samples from trenches might be a result of the storage, clear evidence for this is still missing. These findings call for further investigations. Furthermore, different post-run correction methods for raw data from CRDS measurements are compared showing no significant difference between the three used schemes. These findings are relevant for all studies handling stable isotopes by forming a basis for direct data comparisons from different laboratories.

Representativity of a single firn core

As already mentioned in many studies (e. g. Fisher et al., 1985; Karlöf et al., 2006; Richardson-Näslund, 2004) and also shown in this work, one single profile is not representative for a wider area due to low signal-to-noise ratios and the contribution of non-climatic effects in the isotopic signal; hence, observed variations do not necessarily imply changing climatic conditions. Based on the suggestions from Münch et al. (2016), several firn cores with horizontal distances up to 15 km are analysed around the Kohnen research station. Through the stacking of the individual $\delta^{18}O$ records to one data set (Sections 3.5 and 4.3), the amount of noise is reduced providing an improved estimate of the underlying climate signal. The probability to detect a linear temperature trend by averaging eleven profiles is relatively high assuming a low annual noise variance (Münch et al., 2016). Based on this assumption, the stack is a representative data set for this area for the last 200 years.

Increase of annual accumulation rates

The general annual accumulation rate for the stacked data set increased from about 62 mm w. eq. yr^{-1} in the 19^{th} century to about 78 mm w. eq. yr^{-1} during the last 50

years (Section 4.3) which is an increase by about 25 %. However, the difference of 16 mm w. eq. yr^{-1} is not observed for each core: B47 for example shows much lower annual accumulation rates while B52 indicates higher rates of up to 92 mm w. eq. yr^{-1} in the second half of the 20^{th} century. Thus, large spatial differences in mean annual accumulation rates exist for the area around the Kohnen research station, however, with a general remarkable increase during the last 50 years.

Spatial variability of stable water isotopes in Dronning Maud Land

Precipitation intermittency, post-depositional modifications and surface topography are the main drivers for local variability of stable water isotopes in DML and challenge their climatic interpretation when analysing single profiles. Profiles with a low horizontal spacing do not show significant differences in their mean values (Figure 4.5) and high correlations (Figure 4.10) due to the same noise. However, on a regional scale discrepancies are evident (Figure 4.6).

Warming trend in Dronning Maud Land during the last decades

The main aim of this study was to ascertain whether DML experiences an (anthropogenic) warming trend as suggested by estimates from instrumental observations (Steig et al., 2009). For estimating the temperature change during the last 50 years, the δ^{18}O-T relation has to be known in order to convert isotopic changes to temperature variations in Kelvin. Here, we assume a constant slope of 0.8 ‰ K^{-1} (Oerter et al., 1999). Hence, the observed isotopic change since 1957 corresponds to an increase in temperature of 0.16 °C per decade (Section 4.3, Figure 4.12).

Moreover, a comparison with previously analysed firn cores reaching 1,000 years back in time shows significantly different mean values between the data spanning the range from 1000 to 1950 CE and the new data set until 2012 (Figure 4.14). This finding supports, the hypothesis of changing climatic conditions and recently warming temperatures on parts of the AP. Nevertheless, a deeper understanding about the storage and the imprint of the climate signal into the snow and subsequent alteration is still necessary to reliably quantify the magnitude of temperature change in East Antarctica.

Outlook

The presented data underline the role of spatial averaging to improve the signal-to-noise ratio. Besides a deeper understanding of the imprint of the climate signal in the snow, the role of precipitation and accumulation intermittency is important and has to be investigated in future studies. Comparisons of the season of accumulation with impurity concentrations in ice can give for example a detailed insight in the process of deposition (Freitag et al., 2013b; Hörhold et al., 2012). The effect of storage should also be included in future work. Moreover, isotopic ratios and mean annual accumulation rates are positively correlated, however, changed accumulation rates do not necessarily imply temperature changes. Consequently, learning more

about the archiving process of the temperature signal in the ice core record as well as the timing of accumulation offers the possibility of a more precise statement on a warming trend on the Antarctic continent.

Appendix

A. Analysis methods

Water-Isotope Measurement

AWI Isotope Laboratory Potsdam

Picarro

File: P2017_10_05_Zuhr.csv

Name: Alexandra Zuhr

Rear

1	2	3	4	5	6	7	8	9
10	11	12	13	14	15	16	17	18
19	20	21	22	23	24	25	26	27
28	29	30	31	32	33	34	35	36
37	38	39	40	41	42	43	44	45
46	47	48	49	50	51	52	53	54

Front

1	HGL-1	6	2	HGL-1	6	3	DOME-C1	1	4	DOME-C1	1	5	TD1	4	6	TD1	4	7	CoFi1	8	cofi1	9	DML	4
10	DML	4	11	TD2	1	12	TD2	1	13	S-TD1-4		14	S-JASE-5		15	S-NGT-1		16	S-MXW-4	17	S-TD1-4	18	S-CoFi1	
19	S-DML-4		20	S-JASE-5		21	S-DOME-C1-1		22	S-NGT-1		23	S-KOS1-1		24	S-TD1-4		25	S-TD2-1	26	S-CoFi1	27	S-NGT-1	
28	S-JASE-5		29	DOME-C1	1	30	TD1	4	31	HGL-1	4	32	CoFi1		33	DML	4	34	TD2	1	35	S-TD1-4	36	S-JASE-5	
37	S-NGT-1		38	S-MXW-4		39	S-TD1-4		40	S-CoFi1		41	S-DML-4		42	S-JASE-5		43	S-DOME-C1-1	44	S-NGT-1	45	S-KOS1-1	
46	S-TD1-4		47	S-TD2-1		48	S-CoFi1		49	S-NGT-1		50	S-JASE-5		51	DOME-C1	1	52	TD1	4	53	CoFi1	54	DML	4

Notes:

Figure A.1.: Detailed measurement sequence for the validation measurement between Excel-based and R based post-run correction. The rack contains 54 vials of which 32 are regarded as samples (labeled with 'S') and 22 as reference waters which are separated into three blocks.

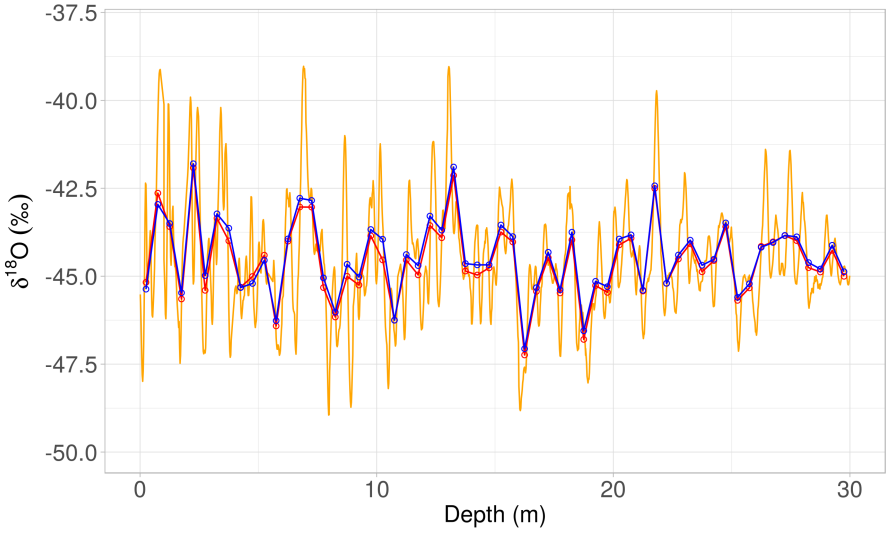

Figure A.2.: Comparison of the 2 cm resolution data set (orange), hereof the 50 cm average (red) and the 50 cm resolution measurement (blue) for B41.

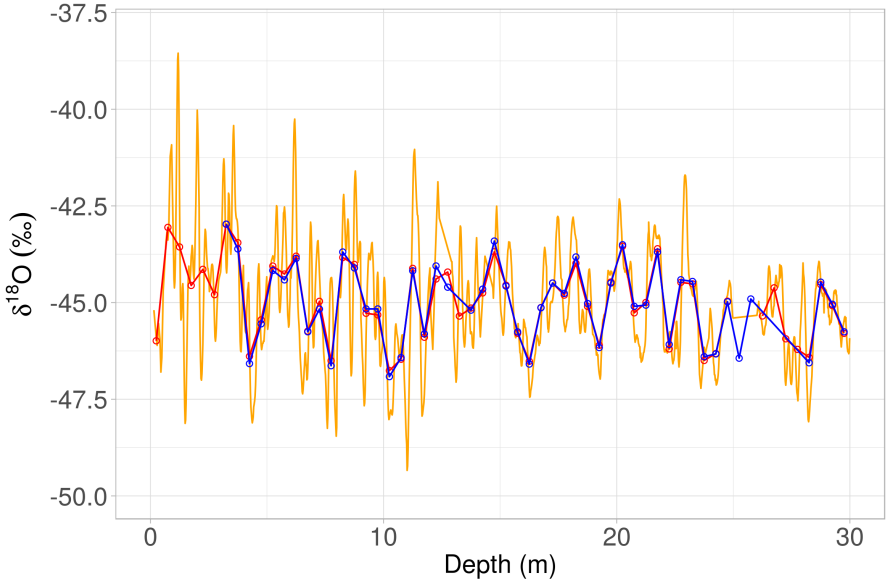

Figure A.3.: Comparison of the 2 cm resolution data set (orange), hereof the 50 cm average (red) and the 50 cm resolution measurement (blue) for B50. Note the missing data in the low resolution measurement (0 - 4 m and 25 - 27 m) as well as missing data in the high resolution data at 13 m which are excluded in the final analysis.

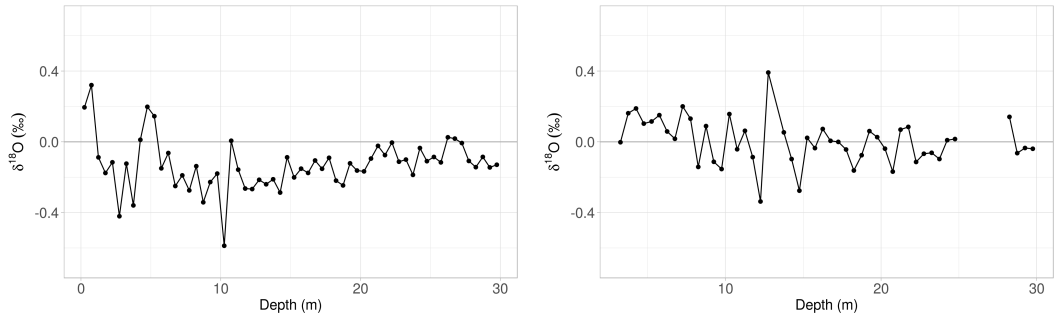

(a) (b)

Figure A.4.: Deviations between high resoultion (2 cm, averaged) and low resolution (50 cm) measurements for a) B41 and b) B50 with a gap between 0 and 4 m as well as 25 and 27 m depth due to missing data.

Table A.1.: Correlations coeffiecients and RMSDs between averaged high resolution data and low resolution data for firn cores B41, B42 and B50. Calculations are preformed for δ^{18}O, δD and d.excess timeseries.

	Correlation			RMSD		
	B41	B42*	B50**	B41	B42*	B50**
δ^{18}O	0.991	0.992	0.992	0.19	0.13	0.13
δD	0.991	0.993	0.991	1.50	1.07	1.19
d.excess	0.962	0.874	0.924	0.36	0.52	0.59

* Depth interval from meter three to five is excluded due to missing data points in the high resolution timeseries.

** Depth interval for meter 13 in the high resolution timesieres is excluded for the same reason.

B. Spatial variability on local to regional scales

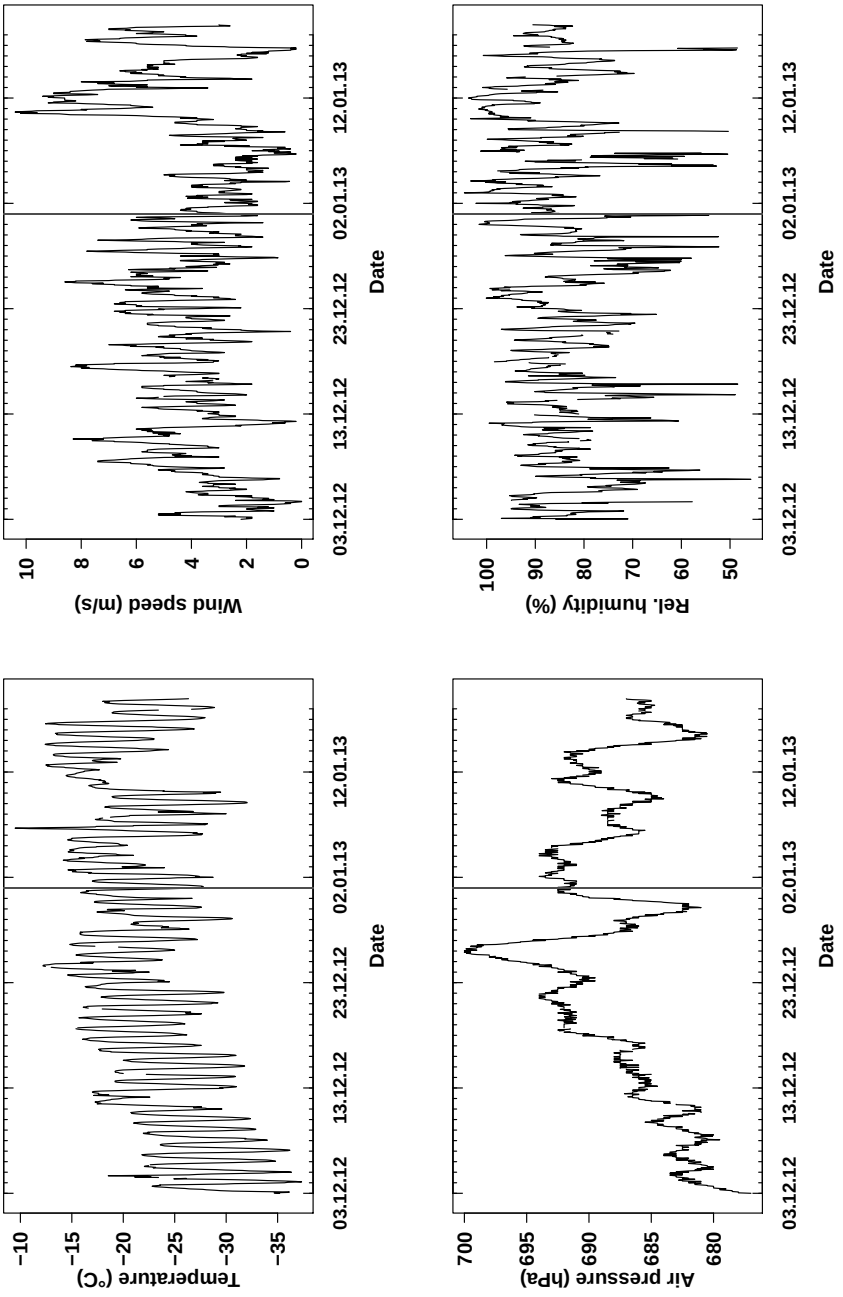

Figure B.1.: Meteorological conditions from AWS 9 for the sampling period of the snow pits KOH1 to KOH8 (03.12.2012 - 18.01.2013). Shown are temperature, wind speed, pressure and relative humidity. The vertical line indicate the turn of the year.

C. Temporal variability of the $\delta^{18}O$ stack

Table C.1.: Horizontal distances (normal font) and elevation differences (in italic), both in meter, between firn cores B31, B32 and B33.

	B31	B32	B33
B33	283.4	187.4	0
B32	116.9	0	*278*
B31	0	*13*	*491*

Bibliography

Bamber, J. L., Gomez-Dans, J. L., and Griggs, J. A. 2009. Antarctic 1 km Digital Elevation Model (DEM) from combined ERS-1 Radar and ICESat Laser Satellite Altimetry, Version 1. *National Snow and Ice Data Center. Boulder, Colorado USA*. doi: http://dx.doi.org/10.5067/H0FQ1KL9NEKM.

Casado, M., Landais, A., Picard, G., Münch, T., Laepple, T., Stenni, B., Dreossi, G., Ekaykin, A., Arnaud, L., Genthon, C., Touzeau, A., Masson-Delmotte, V., and Jouzel, J. 2016. Archival of the water stable isotope signal in East Antarctic ice cores. *The Cryosphere Discuss.* doi: 10.5194/tc-2016-263.

Craig, H. 1961. Standard for Reporting Concentrations of Deuterium and Oxygen-18 in Natural Waters. *Science*, pages 1833–1834. doi: 10.1126/science.133.3467.1833.

Cuffey, K. M. and Paterson, W. S. B. 2010. *The Physics of Glaciers*, volume 4. Academic Press. ISBN 978-0-123-69461-4.

Cuffey, K. M. and Steig, E. J. 1998. Isotopic diffusion in polar firn: implications for interpretation of seasonal climate parameters in ice-core records, with emphasis on central Greenland. *Journal of Glaciology*, 44(147):273–284. doi: 10.1017/S0022143000002616.

Dansgaard, W. 1964. Stable isotopes in precipitation. *Tellus*, 16(4):436–468. doi: 10.3402/tellusa.v16i4.8993.

Delmas, R. J., Kirchner, S., Palais, J. M., and Petit, J. 1992. 1000 years of explosive volcanism recorded at the south pole. *Tellus B*, 44(4):335–350. doi: 10.1034/j.1600-0889.1992.00011.x.

Drücker, C., Wilhelms, F., Oerter, H., Frenzel, A., Gernandt, H., and Miller, H. 2002. Design, transport, construction, and operation of the summer base Kohnen for ice-core drilling in Dronning Maud Land, Antarctica. *Memoirs Natinal Inst. Polar Res.*, 56:302–312.

EPICA community members. 2004. Eight glacial cycles from an Antarctic ice core. *Nature*, 429(6992):623–628. doi: 10.1038/nature02599.

EPICA community members. 2006. One-to-one coupling of glacial climate variability in Greenland and Antarctica. *Nature*, 444(7116):195–198. doi: 10.1038/nature05301.

Fisher, D. A., Reeh, N., and Clausen, H. B. 1985. Stratigraphic Noise in Time Series Derived from Ice Cores. *Annals of Glaciology*, 7(1):76–83. doi: 10.1017/S0260305500005942.

Freitag, J., Kipfstuhl, S., and Laepple, T. 2013a. Core-scale radioscopic imaging: a new method reveals density–calcium link in Antarctic firn. *Journal of Glaciology*, 59(218):1009–1014. doi: 10.3189/2013JoG13J028.

Freitag, J., Kipfstuhl, S., Laepple, T., and Wilhelms, F. 2013b. Impurity-controlled densification: a new model for stratified polar firn. *Journal of Glaciology*, 59(218):1163 – 1169. doi: 10.3189/2013JoG13J042.

Fujita, S., Okuyama, J., Hori, A., and Hondoh, T. 2009. Metamorphism of stratified firn at Dome Fuji, Antarctica: A mechanism for local insolation modulation of gas transport conditions during bubble close off. *Journal of Geophysical Research: Earth Surface*, 114 (F3). doi: 10.1029/2008JF001143.

Fujita, S., Holmlund, P., Andersson, I., Brown, I., Enomoto, H., Fujii, Y., Fujita, K., Fukui, K., Furukawa, T., Hansson, M., Hara, K., Hoshina, Y., Igarashi, M., Iizuka, Y., Imura, S., Ingvander, S., Karlin, T., Motoyama, H., Nakazawa, F., Oerter, H., Sjöberg, L. E., Sugiyama, S., Surdyk, S., Ström, J., Uemura, R., and Wilhelms, F. 2011. Spatial and temporal variability of snow accumulation rate on the East Antarctic ice divide between Dome Fuji and EPICA DML. *The Cryosphere*, 5(4):1057–1081. doi: 10.5194/tc-5-1057-2011.

Gonfiantini, R. 1978. Standards for stable isotope measurements in natural compounds. *Nature*, 271(5645):534–536. doi: 10.1038/271534a0.

Graf, W., Oerter, H., Reinwarth, O., Stichler, W., Wilhelms, F., Miller, H., and Mulvaney, R. 2002. Stable-isotope records from Dronning Maud Land, Antarctica. *Annals of Glaciology*, 35(1):195–201.

Hatvani, I. G., Leuenberger, M., Kohán, B., and Kern, Z. 2017. Geostatistical analysis and isoscape of ice core derived water stable isotope records in an Antarctic macro region. *Polar Science*, 13:22–32. doi: 10.1016/j.polar.2017.04.001.

Herron, M. M. and Langway, C. C., Jr. 1980. Firn Densification: An Empirical Model. *Journal of Glaciology*, 25(93):373–385. doi: 10.3189/S0022143000015239.

Hörhold, M., Kipfstuhl, S., Wilhelms, F., Freitag, J., and Frenzel, A. 2011. The densification of layered polar firn. *Journal of Geophysial Research*, 116(F01001). doi: 10.1029/2009JF001630.

Hörhold, M. W., Laepple, T., Freitag, J., Bigler, M., Fischer, H., and Kipfstuhl, S. 2012. On the impact of impurities on the densification of polar firn. *Earth and Planetary Science Letters*, 325–326:93–99. doi: 10.1016/j.epsl.2011.12.022.

IPCC. 2001. *IPCC Third Assessment Report: Climate Change 2001. Working Group II: Impacts, Adaptation and Vulnerability – 16. Polar Regions (Arctic and Antarctic).* Cambridge University Press, Cambridge, United Kingdom and New York, NY, USA.

IPCC. 2013. *IPCC Fifth Assessment Report: Climate Change 2013: The Physical Science Basis. Contribution of Working Group I to the Fifth Assessment Report of the Intergovernmental Panel on Climate Change.* Cambridge University Press, Cambridge, United Kingdom and New York, NY, USA.

Johnsen, S. J., Clausen, K., H. B. Cuffey, Hoffmann, G., Schwander, J., and Creyts, T. 2000. Diffusion of stable isotopes in polar firn and ice: the isotope effect in firn diffusion. *Physics of Ice Core Records*, pages 121–140.

Jones, J. M., Gille, S. T., Goosse, H., Abram, N. J., Canziani, P. O., Charman, D. J., Clem, K. R., Crosta, X., de Lavergne, C., Eisenman, I., England, M. H., Fogt, R. L., Frankcombe,

L. M., Marshall, G. J., Masson-Delmotte, V., Morrison, A. K., Orsi, A. J., Raphael, M. N., Renwick, J. A., Schneider, D. P., Simpkins, G. R., Steig, E. J., Stenni, B., Swingedouw, D., and Vance, T. R. 2016. Assessing recent trends in high-latitude Southern Hemisphere surface climate. *Nature Climate Change*, 6(10):917–926. doi: 10.1038/nclimate3103.

Jouzel, J. and Merlivat, L. 1984. Deuterium and Oxygen 18 in Precipitation: Modeling of the Isotopic Effects During Snow Formation. *Journal of Geophysical Research: Atmospheres*, 89(D7):11749–11757. doi: 10.1029/JD089iD07p11749.

Jouzel, J., Alley, R. B., Cuffey, K. M., Dansgaard, W., Grootes, P., Hoffmann, G., Johnsen, S. J., Koster, R. D., Peel, D., Shuman, C. A., Stievenard, M., Stuiver, M., and White, J. 1997. Validity of the temperature reconstruction from water isotopes in ice cores. *Journal of Geophysical Research: Oceans*, 102:26471–26487. doi: 10.1029/97JC01283.

Karlöf, L., Winther, J.-G., Isaksson, E., Kohler, J., Pinglot, J. F., Wilhelms, F., Hansson, M., Holmlund, P., Nyman, M., Pettersson, R., Stenberg, M., Thomassen, M. P. A., van der Veen, C., and van de Wal, R. S. W. 2000. A 1500 year record of accumulation at Amundsenisen western Dronning Maud Land, Antarctica, derived from electrical and radioactive measurements on a 120 m ice core. *Journal of Geophysical Research*, 105 (D10):12471–12483. doi: 10.1029/1999JD901119.

Karlöf, L., Isaksson, E., Winther, J.-G., Gundestrup, N., Meijer, H. A., Mulvaney, R., Pourchet, M., Hofstede, C., Lappegard, G., Pettersson, R., van den Broeke, M., and van de Wal, R. S. W. 2005. Accumulation variability over a small area in east Dronning Maud Land, Antarctica, as determined from shallow firn cores and snow pits: some implications for ice-core records. *Journal of Glaciology*, 51(174):343–352.

Karlöf, L., Winebrenner, D. P., and Percival, D. B. October 2006. How representative is a time series derived from a firn core? A study at a low-accumulation site on the Antarctic plateau. *Journal of Geophysical Research*, 111(F04001). doi: 10.1029/2006JF000552.

Kaufmann, P. R., Federer, U., Hutterli, M. A., Bigler, M., Schüpbach, S., Ruth, U., Schmitt, J., and Stocker, T. F. 2008. An Improved Continuous Flow Analysis System for High-Resolution Field Measurements on Ice Cores. *Environmental Science & Technology*, 42 (21):8044–8050. doi: 10.1021/es8007722. PMID: 19031900.

Kerstel, E. and Gianfrani, L. 2008. Advaneds in laser-based isotope ration measurements: selected applications. *Applied Physics B*, 92:439–449. doi: 10.1007/s00340-008-3128-x.

Kerstel, E., van Trigt, R., Dam, N., Reuss, J., and Meijer, H. A. J. 1999. Simultaneous Determination of the $^{2}H/^{1}H$, $^{17}O/^{16}O$, and $^{18}O/^{16}O$ Isotope Abundance Ratios in Water by Means of Laser Spectrometry. *Analytical Chemistry*, 71(23):5297–5303. doi: 10.1021/ac990621e.

Laepple, T., Hörhold, M., Münch, T., Freitag, J., Wegner, A., and Kipfstuhl, S. 2016. Layering of surface snow and firn at Kohnen Station, Antarctica: Noise or seasonal signal? *Journal of Geophysical Research: Earth Surface*, 121(10):1849–1860. doi: 10.1002/2016JF003919.

Laepple, T., Münch, T., Casado, M., Hoerhold, M., Landais, A., and Kipfstuhl, S. 2017. On the similarity and apparent cycles of isotopic variations in East Antarctic snow-pits. *The Cryosphere Discussions*. doi: 10.5194/tc-2017-199.

Maeno, N. and Ebinuma, T. 1983. Pressure sintering of ice and its implication to the densification of snow at polar glaciers and ice sheets. *The Journal of Physical Chemistry*, 87(21):4103–4110. doi: 10.1021/j100244a023.

Marcott, S. A., Shakun, J. D., Clark, P. U., and Mix, A. C. 2013. A Reconstruction of Regional and Global Temperature for the Past 11,300 Years. *Science*, 339(6124):1198–1201. doi: 10.1126/science.1228026.

Masson-Delmotte, V., Hou, S., Ekaykin, A., Jouzel, J., Aristarain, A., Bernardo, R. T., Bromwich, D., Cattani, O., Delmotte, M., Falourd, S., Frezzotti, M., Gallée, H., Genoni, L., Isaksson, E., Landais, A., Helsen, M. M., Hoffmann, G., Lopez, J., Morgan, V., Motoyama, H., Noone, D., Oerter, H., Petit, J. R., Royer, A., Uemura, R., Schmidt, G. A., Schlosser, E., Simões, J. C., Steig, E. J., Stenni, B., Stievenard, M., van den Broeke, M. R., van de Wal, R. S. W., van de Berg, W. J., Vimeu, F., and White, J. W. C. 2008. A Review of Antarctic Surface Snow Isotopic Composition: Observations, Atmospheric Circulation, and Isotopic Modeling. *Journal of Climate*, 21(13):3359–3387. doi: 10.1175/2007JCLI2139.1.

Masson-Delmotte, V., Steen-Larsen, H. C., Ortega, P., Swingedouw, D., Popp, T., Vinther, B. M., Oerter, H., Sveinbjornsdottir, A. E., Gudlaugsdottir, H., Box, J. E., Falourd, S., Fettweis, X., Gallée, H., Garnier, E., Gkinis, V., Jouzel, J., Landais, A., Minster, B., Paradis, N., Orsi, A., Risi, C., Werner, M., and White, J. W. C. 2015. Recent changes in north-west Greenland climate documented by NEEM shallow ice core data and simulations, and implications for past-temperature reconstructions. *The Cryosphere*, 9(4):1481–1504. doi: 10.5194/tc-9-1481-2015.

McConnell, J. R., Lamorey, G. W., Lambert, S. W., and Taylor, K. C. 2002. Continuous Ice-Core Chemical Analyses Using Inductively Coupled Plasma Mass Spectrometry. *Environmental Science & Technology*, 36(1):7–11. doi: 10.1021/es011088z.

Münch, T. piccr, 2017. URL `https://bitbucket.org/ecus/piccr`.

Münch, T., Kipfstuhl, S., Freitag, J., Meyer, H., and Laepple, T. 2016. Regional climate signal vs. local noise: a two-dimensional view of water isotopes in Antarctic firn at Kohnen Station, Dronning Maud Land. *Clim. Past*, 12(7):1565–1581. doi: 10.5194/cp-12-1565-2016.

Münch, T., Kipfstuhl, S., Freitag, J., Meyer, H., and Laepple, T. 2017. Constraints on post-depositional isotope modifications in East Antarctic firn from analysing temporal changes of isotope profiles. *The Cryosphere*, 11(5):2175–2188. doi: 10.5194/tc-11-2175-2017.

National Research Council. 2006. *Surface Temperature Reconstructions for the Last 2,000 Years*. The National Academies Press, Washington, DC. ISBN 978-0-309-10225-4. doi: 10.17226/11676.

Nishimura, H., Maeno, N., and Satow, K. 1983. Initial stage of densification of snow in Mizhuho plateau, Antarctica. *Memoirs of National Institute of Polar Research*.

Oerter, H., Graf, W., Wilhelms, F., Minikin, A., and Miller, H. 1999. Accumulation studies on Amundsenisen, Dronning Maud Land, Antarctica, by means of tritium, dielectric profiling and stable-isotope measurements: first results from the 1995–96 and 1996–97 field seasons. *Annals of Glaciology*, 29(1):1–9. doi: 10.3189/172756499781820914.

Oerter, H., Wilhelms, F., Jung-Rothenhäusler, F., Göktas, F., Miller, H., Graf, W., and Sommer, S. 2000. Accumulation rates in Dronning Maud Land, Antarctica, as revealed by dielectric-profiling measurements of shallow firn cores. *Annals of Glaciology*, 30(1): 27–34. doi: 10.1038/nclimate2293.

Percival, D. B. and Walden, A. T. 1993. *Spectral Analysis for Physical Applications: Multitaper and Conventional Univariate Techniques*. Cambridge University Press, Cambridge, UK. ISBN 978-0-511-62276-2.

Piarro Inc. 2018. PICARRO: Cavity Ring-Down Spectroscopy (CRDS). URL `https://www.picarro.com/technology/cavity_ring_down_spectroscopy`.

Picarro Inc. 2018. PICARRO: Measure water (H_2O) isotopes in solids, liquids and vapor. URL `https://www.picarro.com/products_solutions/peripherals/for_h2o/ih2o_solids_liquids_and_vapor`.

R Core Team. *R: A Language and Environment for Statistical Computing*. R Foundation for Statistical Computing, Vienna, Austria, 2017.

Reijmer, C. H. 2001. *Antarctic Meteorology, a study with automatic weather stations*. PhD thesis, University of Utrecht.

Reijmer, C. H. and van den Broeke, M. R. 2003. Temporal and spatial variability of the surface mass balance in Dronning Maud Land, Antarctica, as derived from automatic weather stations. *Journal of Glaciology*, 49(167):512–520.

Richardson, C., Aarholt, E., Hamran, S., Holmlund, P., and Isaksson, E. 1997. Spatial distribution of snow in western Dronning Maud Land, East Antarctica, mapped by a ground-based snow radar. *Journal of Geophysical Research: Solid Earth*, 102(B9):20343–20353. doi: 10.1029/97JB01441.

Richardson-Näslund, C. 2004. Spatial characteristics of snow accumulation in Dronning Maud Land, Antarctica. *Global and Planetary Change*, 42:31–43. doi: 10.1016/j.gloplacha.2003.11.009.

Schilt, A., Baumgartner, M., Blunier, T., Schwander, J., Spahni, R., Fischer, H., and Stocker, T. F. 2010. Glacial–interglacial and millennial-scale variations in the atmospheric nitrous oxide concentration during the last 800,000 years. *Quaternary Science Reviews*, 29(1):182–192. doi: https://doi.org/10.1016/j.quascirev.2009.03.011. Climate of the Last Million Years: New Insights from EPICA and Other Records.

Schlosser, E., Manning, K. W., Powers, J. G., Duda, M. G., Birnbaum, G., and Fujita, K. 2010. Characteristics of high-precipitation events in Dronning Maud Land, Antarctica. *Journal of Geophysical Research: Atmospheres*, 115:D14107. doi: 10.1029/2009JD013410.

Schneider, D. P. and Steig, E. J. 2008. Ice cores record significant 1940s Antarctic warmth related to tropical climate variability. *Proceedings of the National Academy of Sciences*, 34:12154–12158. doi: 10.1073/pnas.0803627105.

Sigl, M., McConnel, J. R., Toohey, M., Curran, M., Das, S. B., Edwards, R., Isaksson, E., Kawamura, K., Kipfstuhl, S., Krüger, K., Layman, L., Maselli, O. J., Motizuuki, Y., Motoyama, H., Pasteris, D. R., and Severi, M. 2014. Insights from Antarctica on volcanic forcing during the Common Era. *Nature Climate Change*, 4:693–697.

Sommer, S., Appenzeller, C., Röthlisberger, R., Hutterli, M. A., Stauffer, B., Wagenbach, D., Oerter, H., Wilhelms, F., Miller, H., and Mulvaney, R. 2000. Glacio-chemical study spanning the past 2 kyr on three ice cores from Dronning Maud Land, Antarctica: 1. Annually resolved accumulation rates. *Journal of Geophysical Research: Atmospheres*, 105(D24):29411–29421. doi: 10.1029/2000JD900449.

Steig, E. J., Schneider, D. P., Rutherford, S. D., Mann, M. E., Comiso, J. C., and Shindell, D. T. 2009. Warming of the Antarctic ice-sheet surface since the 1957 International Geophysical Year. *Nature*, 457(7228):459–462. doi: 10.1038/nature07669.

Talalay, P. G. 2016. *Mechanical Ice Drilling Technology*, volume 1. Springer. ISBN 978-981-10-0559-6.

Touzeau, A., Landais, A., Stenni, B., Uemura, R., Fukui, K., Fujita, S., Guilbaud, S., Ekaykin, A., Casado, M., Barkan, E., Luz, B., Magand, O., Teste, G., Le Meur, E., Baroni, M., Savarino, J., Bourgeois, I., and Risi, C. 2016. Acquisition of isotopic composition for surface snow in East Antarctica and the links to climatic parameters. *The Cryosphere*, 10(2):837–852. doi: 10.5194/tc-10-837-2016.

van Geldern, R. and Barth, J. 2012. Optimization of instrument setup and post-run corrections for oxygen and hydrogen stable isotope measurements of water by isotope ratio infrared spectroscopy (IRIS). *Limnology and Oceanography: Methods*, 10:1024–1036. doi: 10.4319/lom.2012.10.1024.

Vimeux, F., Masson, V., Delaygue, G., Jouzel, J., Petit, J. R., and Stievenard, M. 2001. A 420,000 year deuterium excess record from East Antarctica: Information on past changes in the origin of precipitation at Vostok. *Journal of Geophysical Research: Atmospheres*, 106(D23). doi: 10.1029/2001JD900076.

Weißbach, S., Wegner, A., Opel, T., Oerter, H., Vinther, B. M., and Kipfstuhl, S. 2016. Spatial and temporal oxygen isotope variability in northern Greenland – implications for a new climate record over the past millennium. *Clim. Past*, 12(2):171–188. doi: 10.5194/cp-12-171-2016.

Whillans, I. M. and Grootes, P. M. 1985. Isotopic diffusion in cold snow and firn. *Journal of Geophysical Research: Atmospheres*, 90(D2):3910–3918. doi: 10.1029/JD090iD02p03910.

Danksagung

Hiermit möchte ich mich bei all denjenigen bedanken, die mich während meiner Masterarbeit unterstützt und mir die Anfertigung ermöglicht haben.

Lieber Herr Prof. Jacobeit, besonders möchte ich mich bei Ihnen dafür bedanken, dass Sie mir als Erstgutachter die Anfertigung dieser Arbeit ermöglicht haben.

Lieber Thomas, herzlichen Dank für Deine ausdauernde Betreuung, Unterstützung und viele anregende Diskussionen während der letzten Monate.

Lieber Thom, herzlichen Dank für Deine Betreuung und für die Möglichkeit mich in ein neues, spannendes Gebiet einarbeiten zu dürfen.

Ebenfalls möchte ich mich bei der gesamten ECUS/SPACE Arbeitsgruppe bedanken für die spannende Zeit, lehrreiche Diskussionen, insbesondere zu Spektren, und das angenehme Arbeitsklima.

Liebe Maria, lieber Sepp, vielen Dank für die Einführung, die Betreuung und die Unterstützung im Eislabor.

Weiterhin möchte ich dem Team des Isotopenlabors, besonders Hanno, Mikaela und Kirstin, danken für die nette Betreuung und die fachliche Kompetenz während meiner Zeit im Labor.

Liebe Ines, lieber Patrick, bei euch möchte ich mich bedanken für anregende Gespräche, das Korrekturlesen meiner Arbeit und gegenseitige Motivationszusprechungen.

Meinen Eltern möchte ich danken für die großartige Unterstützung während meines gesamten Studiums.

Besonders möchte ich mich bei meinem Freund Jonas bedanken. Danke, dass Du mich während der gesamten Zeit unterstützt und immer wieder motiviert hast.

Eidesstattliche Erklärung

Ich versichere, dass ich die vorliegende Arbeit ohne fremde Hilfe und ohne Benutzung anderer als der angegebenen Quellen angefertigt habe, und dass die Arbeit in gleicher oder ähnlicher Form noch keiner anderen Prüfungsbehörde vorgelegen hat. Alle Ausführungen der Arbeit, die wörtlich oder sinngemäß übernommen wurden, sind als solche gekennzeichnet.

Potsdam, den 20. April 2018